*Master Thesis:* ***March-September 2012***

# Study of the Thermo-mechanical behaviour of an innovative multi-layered ceramic-based nuclear fuel cladding


***Author:*** ***HUGUET GARCIA, Juan Fco***

*juan.huguet@gmail.com*

***Referee:*** ***RUBIOLO, Pablo***

*pablo.rubiolo@phelma.grenoble-inp.fr*

***Tutor:*** ***ZABIEGO, Maxime***

*CEA/DEN/CAD/DEC/SESC/LC2I*
*Bat 315, Pièce 213*
*CEA Cadarache*
*F-13108 Saint-Paul-lez-Durance*
*maxime.zabiego@cea.fr*

***Host institution & laboratory:***
*Commisariat à l'Energie Atomique et aux Energies Alternatives (CEA-Cadarache)*

*CEA/DEN/CAD/DEC/SESC/LC2I*

# [Acknowledgement]

Thanks to Maxime Zabiego, internship tutor, for all his advices, patience and dedicated time. It has been a real pleasure to be under the tutelage of such a great person in both, professional and personal aspect. Thanks for the opportunity to work in such a great environment.

Thanks to Eric Brunon and Thomas Helfer, for their immense and valuable help, for all the shared knowledge and the patience to teach me during the internship. It has been really a good experience to cooperate with high level researchers like you two.

Thanks to Vincent Marelle for his help with `Alcyone` and to Etienne Castelier for providing the mechanical models used in this study.

Thanks to Sylvie Pillon, laboratory's head, for her welcome into the LC2I team. My best wishes for your new professional phase.

Thanks to all the LC2I. All of you made me feel like one more in the team and made from this internship an unforgettable experience.

# [Table of Contents]

## [List of Tables]



## [List of Figures]

## [Glossary]

BOL: Beginning Of Life

BWR: Boiling Water Reactor

CEA: Commisariat à l'Energie Atomique et aux Energies Alternatives

CMC: Ceramic Matrix Composite

CVD: Chemical Vapor Deposition

CVI: Chemical Vapor Infiltration

DPA: displacement per atom. A quantitative measure of the amount of irradiation damage a material has undergone.

E: Young Modulus

EIT: European Institute of Innovation and Technology

EOL: End Of Life

ETSEIB: Escola Tecnica Superior d' Enginyeria Industrial de Barcelona

LWR: Light Water Reactor

MCS: Matrix Cracking Stress

NPP: Nuclear Power Plant

PCMI: Pellet Cladding Mechanical Interaction

PWR: Pressurized Water Reactor

PyC: Pyrolithic Carbon

RIA: Reactivity Initiated Accident

SiC: Silicon Carbide

UTS: Ultimate Tensile Stress

# 1. CEA-Cadarache

The CEA is the French Alternative Energies and Atomic Energy Commission (Commissariat à l'énergie atomique et aux énergies alternatives). It is a public body established in October 1945 by General de Gaulle. A leader in research, development and innovation, the CEA mission statement has two main objectives: To become the leading technological research organization in Europe and to ensure that the nuclear deterrent remains effective in the future.

The CEA is based in ten research centres in France, each specializing in specific fields. The laboratories are located in the Paris region, the Rhône-Alpes, the Rhône valley, the Provence-Alpes-Côte d'Azur region, Aquitaine, Central France and Burgundy.

The Cadarache facility at the Provence-Alpes-Côte d'Azur region is one of the largest nuclear research sites in Europe, hosting 21 fixed nuclear installations, including reactors, waste stockpiling and recycling facilities and research centres. It employs over 4,500 people, and approximately 350 students and foreign collaborators carry out research in the facility's laboratories.

CEA-Cadarache's host laboratory is the LC2I (Conception and Irradiation Laboratory for Innovative Nuclear Fuels). This laboratory, directed by Mme Sylvie Pillon, is dependant of the SESC (Fuel's Behavior Study and Simulation Service), itself included in the DEC (Fuel's Study Department). DEC belongs do the DEN (Energy Nuclear Direction)

LC2I mission is to conceive, to dimension and to qualify fuel assemblies for fast neutron nuclear reactors and to design and perform in-core radiation experiences.

The team is composed by 14 engineers, one technician and one secretary. The specialities are mainly thermo-mechanics and thermo-hydraulics but with extended knowledge in various fields from materials to computer assisted conception, all merging in the nuclear engineering field.

# 2. Overview

Nuclear fuel claddings are the most demanded elements in a Nuclear Power Plant (NPP). They have to be capable to withstand with the different loads during its in-core residence while ensuring a coolable geometry and the retention of the created fission products.

## 2.1 In-core cladding solicitations

During its residence in the reactor, the nuclear fuel cladding is under different mechanical loads. Depending on the source they can be classified in:

**Primary stresses**: Imposed by the differential of pressure between the coolant and the inner gas. In nominal operation, the imposed external pressure is in the order of 15.5 MPa and the interior varies from 1.5-3 MPa at BOL to 12 MPa at EOL due to

fission gases release. During transients, internal pressure increases the load as it follows an approximated linear trend with the temperature ($P \cdot V = n \cdot R \cdot T$). These stresses are not able to be relaxed by strain or material damage.

**Secondary stresses:** These are caused by differential deformations within the material caused by thermal gradient across the cladding.

These stresses are able to be relaxed by different mechanisms.

In metallic alloys claddings the main secondary stress relaxation mechanism relies on the cladding´s ability to deform in a visco-elastic or visco-plastic form.
This deformation, called creep, has slows kinetics and takes place in several weeks while the thermal differential deformations take place quasi instantly. This implies that at BOL the cladding will suffer the stresses until the creep appears.
Also, in case of a power shutdown, the thermal gradient disappears and thus the thermal stresses. In this situation, the creep mechanism produces equal stresses but with contrary sign over the cladding that those which relaxed during nominal operation.

In the case of CMC claddings creep is almost negligible. Nevertheless, another relax mechanism appears. SiC swells under irradiation[1]. Due to its dependence with the temperature, differential swelling across the cladding compensates the thermal stresses as the swelling gradient is opposed to the thermal expansion one. Also stresses are restored in case of power shutdown as the thermal gradient disappears.

Due to the degradation of $SiC_f$/SiC heat transfer (from 20 to 5 W/m/K) (Stempien, Carpenter, Kohse, & Kazimi, 2011) secondary stresses may have an important impact on the cladding during nominal and accidental power transients.

**Pseudo-primary stresses[2]:** Gap closure is achieved due the volumetric expansion of the fuel producing stresses over the inner face of the cladding. Pellet-Cladding contact can be divided in two categories depending on which phenomenon is leading the interaction:

1. *Steady PCMI*: The contact is driven by the fission products swelling along the irradiation cycle. The interaction slow kinetics may allow the relaxation of the load by fuel's creep.
2. *Transient PCMI*: The contact is driven by the thermal expansion of the fuel pellet during a power transient. During power transients PCMI may become a major source of stresses. The interaction between the cladding and the fuel pellet happens in a small time scale, as the fuel expansion kinetics is driven by thermal expansion rather than irradiation swelling. This type of load is unlikely to be relaxed and the intensity of the interaction depends on many parameters, mainly the fuel deformation and the contact conditions between fuel and cladding.

[1] SiC swelling depends on both, temperature and fluence. $\phi_0 = 3.396 \cdot 10^{24}$ n/m$^2$
$S(T,\phi) = 4 \cdot \exp(-T[^oC]/370) \cdot (1 - \exp(-\phi/\phi_0))$ [vol %]
[2] Pseudo-primary stresses are potentially relaxable by fuel deformation or fuel damage.

## 2.2 From Zirconium alloys to Ceramic Claddings

In the lasts 50 years, zirconium alloys have been widely used as fuel cladding materials. Nevertheless their fair results, problems with these alloys have been noticed and studied during their service allowing some fair characterisation of their strengths and weaknesses.
The main drawbacks associated to zirconium alloys that limit their in-core residence are (cf. Annex 1 ):

- Exothermal oxidation at high temperatures
- Decrease of their mechanical properties
  - Due to radiation exposure: Embrittlement
  - Long term corrosion: Creation of $ZrO_2$ Oxide layer
- Creep: Clad ballooning can lead to coolant flow restriction and fuel damage.

Even though Zirconium alloys improvements during the lasts years allow higher discharge rates, SiC-based claddings have been proposed to solve their limitations.

SiC chemical stability at high temperatures, resistance to the irradiation damage, low creep and elevated ultimate temperature are their key points to use them as new cladding materials.

In opposition to metallic alloys, ceramic materials may present brittle behaviour with catastrophic failure. This implies that monolithic SiC-based claddings are unsuitable as nuclear fuel cladding as they cannot be used as structural materials.

SiC-based composites have the advantage over monolithic SiC of having a pseudo-ductile fracture. Fracture toughness values on the order of 20 $MPa \cdot m^{0.5}$ have been achieved conferring to the composite a graceful failure mode even at high temperatures. SiCf/SiC mechanical properties are highly dependent on the fibres disposition, braiding or filamentary winding, and the manufacturing process.(cf. Annex 2)

## 2.3 Ceramic cladding designs

Although SiC-based composites are more likable to withstand mechanical loads than monolithic SiC, both materials have manufacturing defects, porosity and micro-cracks. Thus, monolayer ceramic claddings do not grant leak-tightness and multi-layered claddings are proposed.

Previous studies over different multi-layered cladding designs have been carried out to determine their viability as nuclear fuel claddings.

### 2.3.1 Duplex & Triplex concept: *SiC-[SiC$_f$/SiC] & SiC-[SiC$_f$/SiC]-SiC*

This design, proposed by American research teams, may consist in two (*Duplex*) or three (*Triplex*) consecutive SiC layers (cf. Figure 1), comprising: (Feinroth & Hao, 2006)

- A first layer of monolithic SiC. Provides a fission gas containment barrier [20]
- A second composite layer: SiC fibres embedded in a SiC matrix. Gives to the tube the mechanical characteristics needed, namely pseudo-plasticity [22]
- A third layer of monolithic SiC. to give some additional protection against chemical attack and corrosion [24] *(only for Triplex)*

Despite several benefits relying on the SiC properties are present in this design, it presents some drawbacks.

As it's a full ceramic cladding, to maintain the leak-tightness of the cladding, the ensemble is forced to work under compression.

Nowadays manufacturing capabilities to mass product monolithic SiC are only up to 2.5 meters, and the variability introduced by different methods of manufacture effect is not well characterized. This is in compromise with the length of current LWR fuel rods, about 4 meters. (Lahoda, Johnson, & Ray, 2011).

As it is a fully ceramic cladding, once the loads overpass the elastic regime of SiC-based composite, the leak-tightness is not maintained: pseudo-plastic behaviour of $SiC_f$/SiC comes from micro-cracking of the ceramic matrix of the composite allowing fission gas release.

The lack bonding methods for the upper and bottom end plugs which can grant their leak tightness are presently a major source of concern for this design. (Stempien, Carpenter, Kohse, & Kazimi, 2011)

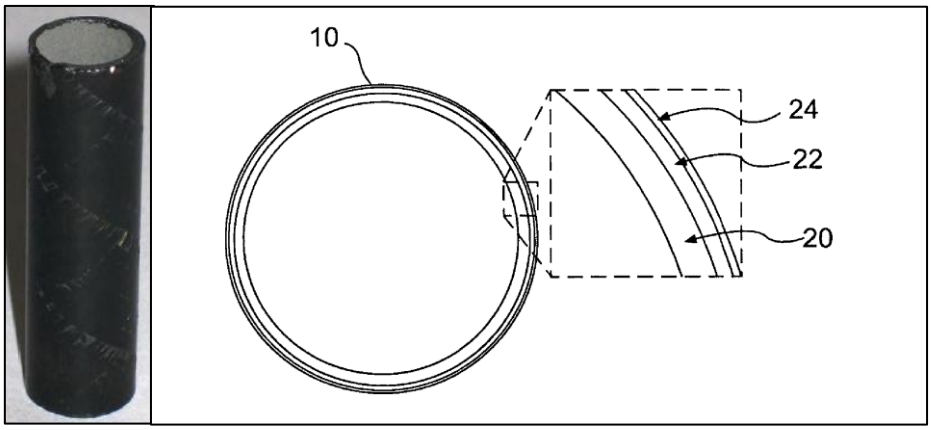


**Figure 1. TRIPLEX USA patent drawing and manufactured tube.**

### 2.3.2 *Sandwich* design. CMC-METAL-CMC

Keeping in mind the advantages of a ceramic cladding and the drawbacks of the *Triplex* concept, the CEA research team has proposed their own multi-layer design, called *Sandwich*.

This design may consist in three consecutive layers:

- $SiC_f$/ SiC inner layer.

- Thin central metallic layer, considering refractory metals or alloys as different options. Niobium, Tantalum, Tungsten and its alloys are being considered as an option.
- $SiC_f$/ SiC outer layer.

The substitution of the monolithic SiC by a metallic layer is supposed to handle the main drawbacks caused with the Duplex/Triplex designs:

- Available manufacture methods for the needed clad lengths.
- Increase of the hermetic domain beyond the CMC elastic regime. The metallic central layer enlarges the useful domain as it maintains the clad leak-tightness when ceramic matrix micro-cracking happens.
- End-cap bonding: The metallic central layer allows welding. The proposed method is to leave uncovered the upper and the bottom part of the multi-layered tube discovering the metallic layer where the end-caps would be placed.

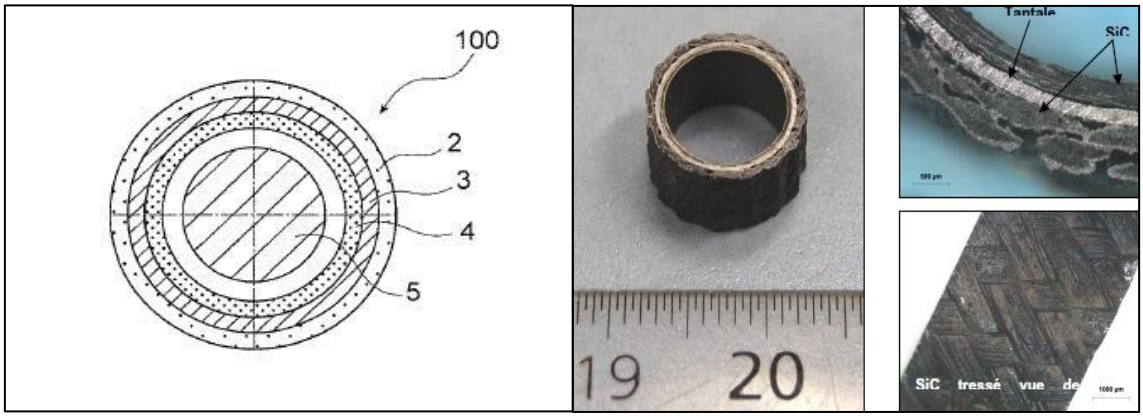


Figure 2. SANDWICH French patent design and prototype

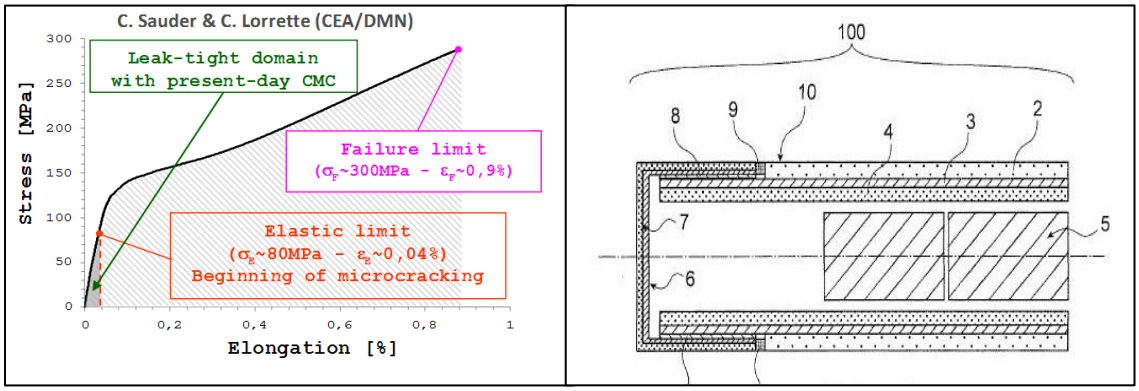


Figure 3. SANDWICH theoretical hermetic domain & end-cap detail.

## 2.4 CMC claddings studies

SiC-based ceramic designs are devoted to replace zircalloy claddings pursuing complementary objectives: Increasing fuels performance (American *Triplex)*, such as burn-up; and improving safety (CEA *Sandwich)*, such as resistance to undesired power transients like reactivity initiated accidents. (RIAs)

Even though their possible advantages, their viability to replace zircalloy claddings is still in a preliminary stage of study, which is not yet conclusive.

Empirical and computational studies on Triplex have been performed. To test their viability under simulated PWR conditions, irradiated samples have been compared to non-irradiated samples. Also SiC-based cladding computer simulations to characterise the PCMI have been performed with FRAPCON, a conservative steady-state fuel rod code for LWR, by using an average monolayer representing the multi-layered structure. (Stempien, Carpenter, Kohse, & Kazimi, 2011) (Carpenter, 2006)

MIT conclusions seem to be too optimistic and not enough critic with potential flaws of the Triplex design:

- The loss of hermeticity during operation is neglected.
- There is no characterisation of the thermal stresses effect during neither nominal nor accidental power transients.
- Interaction between fuel and cladding appear to be weak in terms of the impact over the ceramic claddings as the characterisation made has too many uncertainties due to the lack of a specific tool and the simplifications made.

Although simple analytical studies may allow having an order of magnitude of the loads, the calculus of the constraints with computational methods will be completely necessary to manage more complex and realistic cases.

CEA's research about multi-layered cladding is centred in the development of a tool capable to manage the characterisation of non-conventional geometries and materials under PWR conditions, namely `licos 1.1`.

As `licos 1.1` is under development there are still some features that need to be implemented. Meanwhile, boundary conditions, mainly the internal pressure and the external temperature of the fuel rod, will be generated by using `Alcyone 1.3`. `Alcyone 1.3` is the CEA's reference code for PWR studies.

Previous CEA studies have been performed using this methodology and Sandwich cladding has been characterized under nominal conditions.(cf. Annex 7).

Nevertheless, results obtained are very preliminary and the poor characterisation of the fuel and metallic liner behaviour also neglect the impact of the power transients and the PCMI over the cladding.

The aim of this study is to create a reference case for `licos 1.1`, exploring its capabilities and limitations, to highlight *Sandwich* response to possible limiting phenomena:

- Power transients: How do secondary stresses affect to *Sandwich* clad under nominal or accidental transients.
- PCMI: How does affect pellet-clad interaction to the integrity of the cladding.

As there is no stress criterion for SiC-based composites, no quantitative analysis can be performed and results will be compared to the elastic and failure limit of the ceramic layers.

In order evaluate the potential discrepancies due to limitations on the code and to identify the models that should be implemented in the future, `licos` is benchmarked against `Alcyone`.

Once that the reference case is set, *Sandwich* mechanical characterisation is performed by taken into account different SiC types for the inner and outer layer.

# 3. `Licos` and `Alcyone`: CEA's design and conception codes.

## 3.1 `Licos 1.1` & `Alcyone 1.3`

`licos` is an under development application for fuel design. Its main characteristic is that it allows researchers to deal with non-standard geometries which are not covered by other CEA applications and to modify material models in an easy way.

As it intends to cover a wide range of applications and it is in continuous development, some results may differ from `licos` to the reference code.

Main `licos'` limitations for the present studies are that it does not have a thermo-hydraulic model and that fuel modelling phenomena is not mature enough.

*`Alcyone`* is CEA's reference code for the study of the thermo-mechanical and physico-chemical behaviour of the fuel rods under PWR conditions.
`Alcyone` allows to have validated simulations results for 1D multi-slice, commonly called 1.5D calculations, and 3D calculations for various cladding materials and fuels, UO2 and $SiC_f$/SiC inclusive.

Cladding and fuel geometry are fixed in `Alcyone` to fit the requirements of a PWR standard fuel rod.

As the simulation of a multi-layered fuel cladding is not possible with `Alcyone`, the reference code, and `licos` is still under development; the combination of the two codes is necessary to cover the problem of an advanced thermo-mechanical study for a multi-layered fuel clad.

Finally, the inner pressure evolution and the external surface temperature will be calculated by `Alcyone` and exported to `licos`, which can handle the thermo-mechanical computation for the *Sandwich* cladding non-standard geometry.

## 3.2 Benchmark: licos-vs-Alcyone

### 3.2.1 *licos' reference case*

licos computations are totally specified by the user. This issue added to the fact that the code is continuously improving, not only by the developer but by the users, caused that the invested effort and time to create a reference case for a PWR fuel rod with a multi-layered cladding have been more than the previously planned. Many solutions have been tested in order to find the most acceptable input deck. Starting from the input used in the previous analysis different material properties models have been added and/or modified. The final characterisation responds to a more realistic case allowing better understanding of the in-core solicitations and facilitates further and more detailed thermo-mechanical studies.

### 3.2.2 *Alcyone SiC swelling phenomena*

Previous studies of monolayer SiC claddings with Alcyone pointed to an error of computation. One of the first things to do before boarding the *Sandwich* characterisation has been to check this issue. After come test it appear to be that the material law was well implemented but it was some bad management of the data by the code. Finally the error was detected and communicated to the developer. (cf. Annex 6 )

### 3.2.3 *Material Models*

Table 1 shows the different modified material models..

**Table 1 List of modified material models**

| Material | Material law |
|---|---|
| $SiC_f/SiC$ | Irradiation Swelling Model[1] |
| | Thermal Conductivity[1] |
| | Thermal Strain[1] |
| | Sigma Failure |
| UO2 | Fuel Gaseous Swelling[2] |

1. (Zabiego, Data for the GFR pin design, 2011) 2. Kriging of Alcyone's gaseous swelling for licos.

### 3.2.4 *Hypothesis of computation*

The final input deck is benchmarked against Alcyone to test its consistence and to detect its limitations.

#### 3.2.4.1 Irradiation History

A simplified irradiation history is used to compare both codes. This irradiation history consists in the linearization of the power between transients based on the FX0GAC/E04/4034 EdF's reference history. Linearization aims to reduce calculus time.

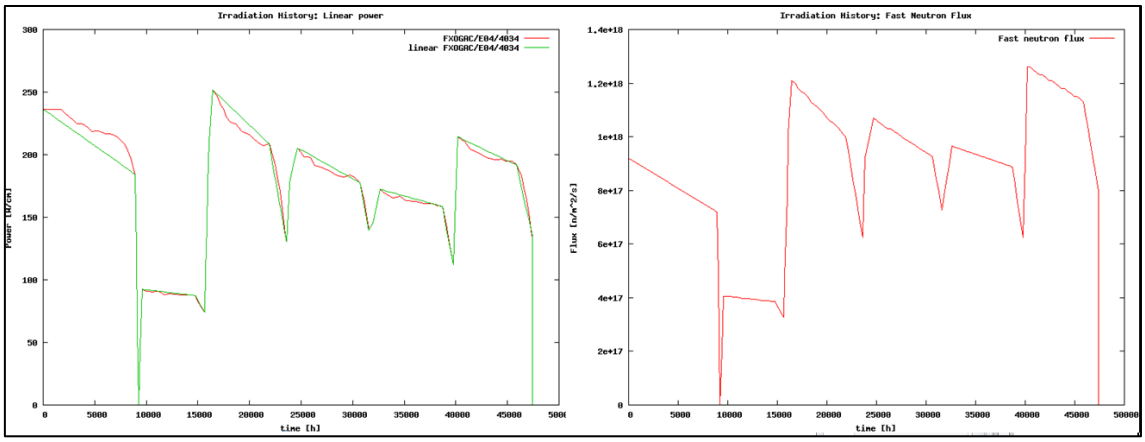


**Figure 4 Irradiation history: Linear Power and neutron flux**

#### 3.2.4.2 Materials models

As up to now, `Alcyone's` SiC irradiation induced swelling model is subject to errors, comparison between the two codes will be performed by using M5 as cladding material. M5 will be the reference material as it has fair characterisation beyond the elastic regime. It will be the metallic liner used in this study although is not compatible with the actual manufacturing processes.

UO2 will be nuclear fuel as is the reference fuel in PWR.

#### 3.2.4.3 Codes' features

As UO2 characterisation is more detailed in `Alcyone` than in `licos`, some features have been disabled in `Alcyone` to avoid a source of discrepancy in the results and to assess the effect of the missing models in `licos`.

UO2's high burn up structure (HBS) and transient gaseous swelling will not be considered in Alcyone computation as these features are not yet implemented in `licos`.

#### 3.2.4.4 Meshing and mechanical hypothesis

`Alcyone` simulation is 1D full fuel rod computation and is run with previous linear power and fast flux-linear power ratio[3]. Rod geometry corresponds to a 30 slice axial discretization of a 200 fuel pellet pin, and 40+6 given radial discretization points of the fuel and the cladding. (MARELLE, 02/2012, p. 9) This configuration is also known as 1.5D simulations to highlight the multi-slice feature.

`Alcyone` calculation is under the hypothesis of axis-symmetrical generalised plane strain and it computes the fuel pellet relocation.

As mentioned in 3.1, `Alcyone`'s full fuel rod and slice's results are used to prepare the input data set for `licos`.

`licos` simulation is 2D-Rθ. This mesh will provide more information about the mechanical response of the cladding and will allow detecting 'hot spots', where stress

[3] Input neutron fast flux data in `Alcyone` is given in [n/m/J]. This unit establishes a relationship between the neutron fast flux and the linear power of the fuel.

concentration may be located and where failure may be originated, especially for PCMI.

`licos` is only calculating 1/16 (22.5º) of the section of the entire fuel rod.

This fuel pellet discretization is to emulate the fuel pellet cracking during the first power transient. Fuel tendency to crack into 8 almost symmetrical parts has been empirically observed and used to simplify the calculation using the resultant planes of symmetry and fracture. (MARELLE, 02/2012, pp. 14-15)

In Figure 5 a representation of the mesh can be observed with the fuel in red, the gas in green and the cladding in blue.

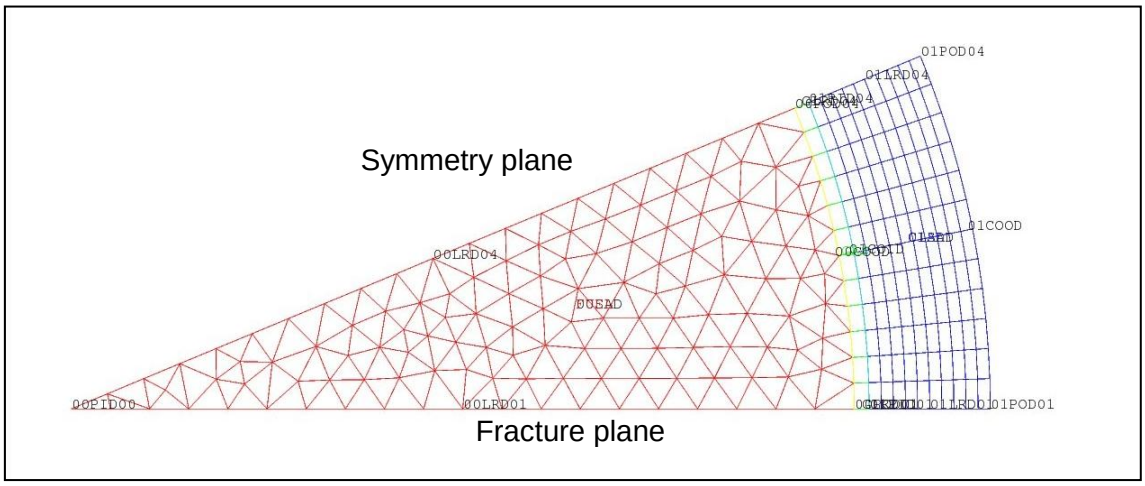


**Figure 5 `licos` 2D-Rθ monolayer mesh. $R_{fuel}$=4.043 mm $R^{ext}_{clad}$=4.745mm $e_{gap}$=77 µm**

`licos` mechanical boundary conditions are specified by the user over the mesh.

Fuel pellet is limited by one fracture plane, over the x axis, and a symmetry line, over the θ direction.

The fracture plane allows the specified frontier to have negative displacements and thus to allow fuel relocation in `licos`. (HELFER, April 2012, p. 79)

#### 3.2.4.5 Internal Pressure and External Temperature

Internal pressure evolution and cladding external temperature are given by the 1.5D simulation of the reference code. In Annex 4Annex 4 the input data for a `licos` computation is shown.

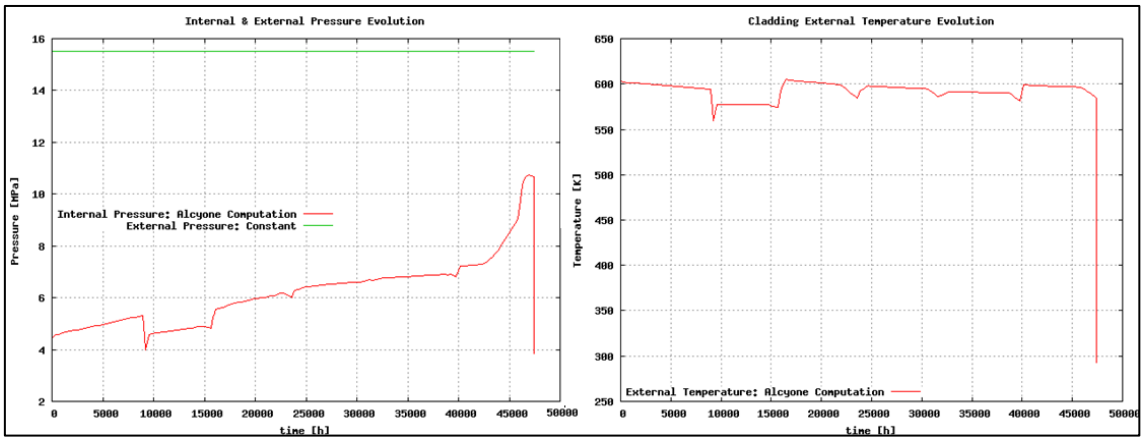


**Figure 6 Internal and external Pressure and external cladding temperature evolutions. `Alcyone` 1.5D computation.**

## *3.3 Burn Up and Temperature evolution*

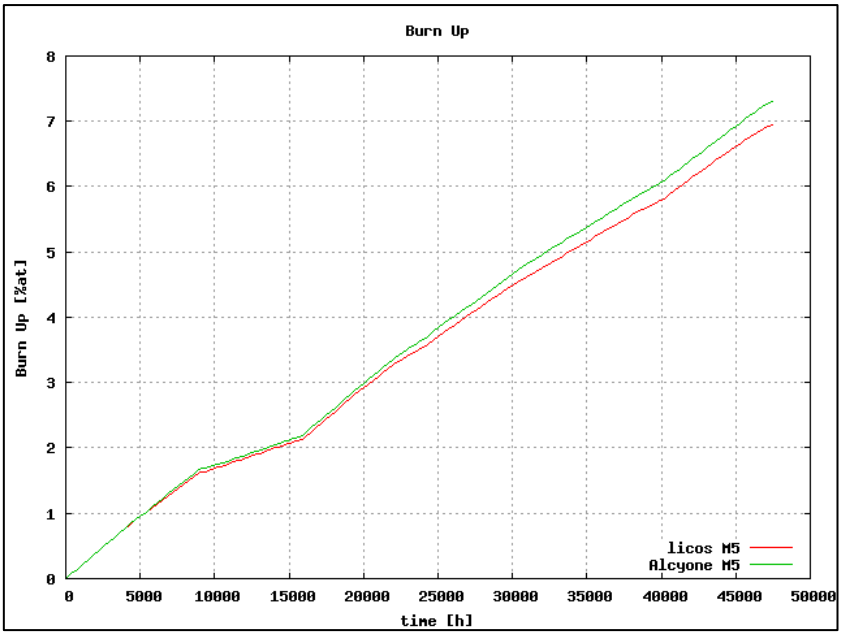


**Figure 7 Fuel centre Burn Up evolution.**

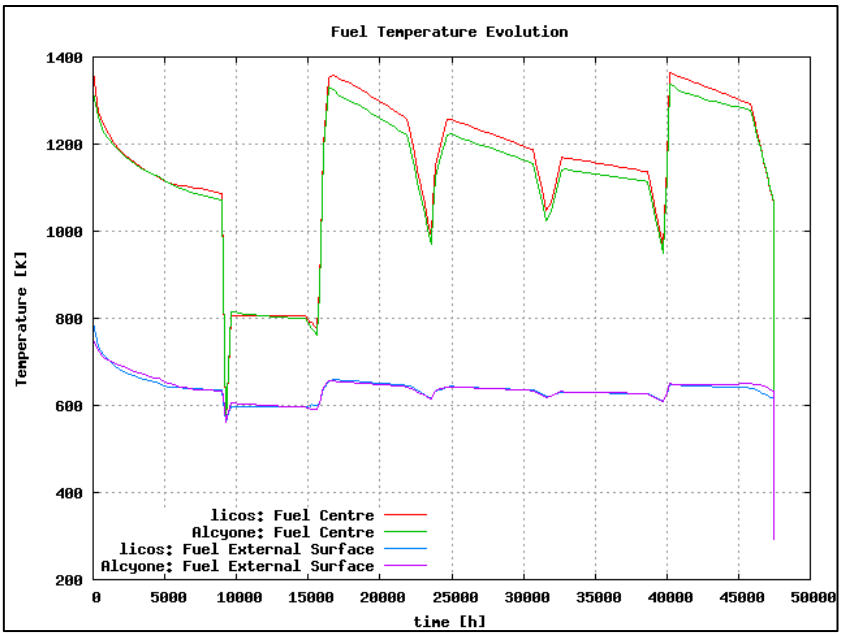


**Figure 8 Comparison of Fuel Temperatures Evolution**

As can be observed in Figure 7 and Figure 8, slight differences appear between the two codes.

Regarding de Burn Up computation, differences in results appear due to the different models of calculations. `Alcyone` model gives two values, the Burn Up of the axial slice and then the local Burn Up, which depends on the first one. This model depends mainly on the linear power and the variation of flux while the `licos` model is mainly using the volumetric power to compute it. (HELFER, April 2012, p. 39) (Meteor V2, 2006, pp. 25-26)

Volumetric power history for `licos` is generated by using results from `Alcyone`, dividing the given linear power at each time by the ideal area of the fuel; this last is calculated with the radius of the pellet at a given time without taking in account relocation. This, added to the different burn up models, explain the observed differences.

Regarding the thermal behaviour, a constant difference of temperature is observed from the third irradiation cycle between `licos and Alcyone.` The external temperatures of the fuel pellet are equal in both codes. This fact shows a good correspondence of the thermal behaviour of the gap and cladding between the two codes and it points out that the observed difference is caused by the thermal behaviour inside the fuel pellet.

As both have implemented the same thermal conductivity (MARELLE, 02/2012, pp. 22-23) this difference is caused by two main facts: The difference in the burn up computation, as thermal conductivity in both codes depends on the Burn Up, and the power distribution inside the fuel pellet. This distribution is constant in `licos` while in `Alcyone` it depends on the radial and axial position. (Meteor V2, 2006)

## 3.4 Radial Evolution

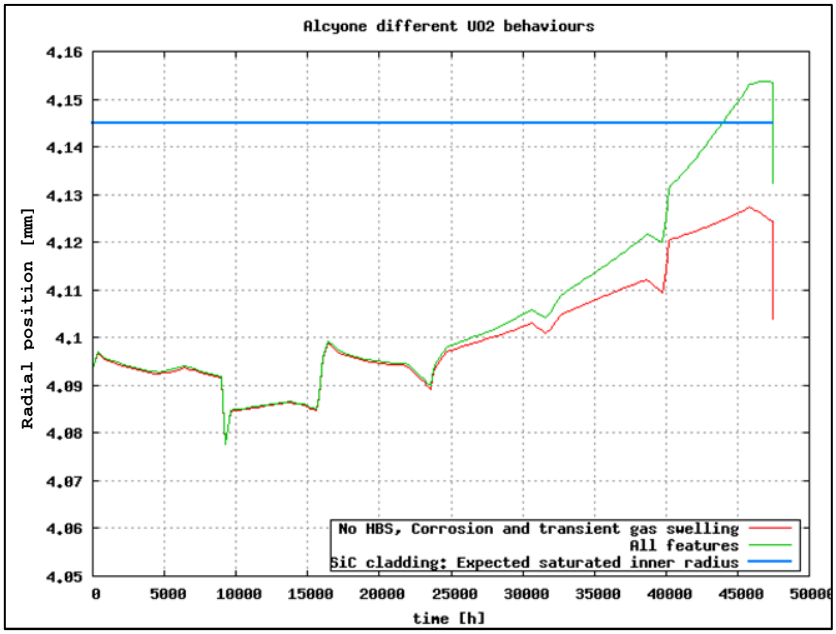


**Figure 9 `Alcyone` different UO2 features. SiC final radius : Rini *(1+(Ssat=4·e$^{-T/370}$))**

As commented, some features of UO2 characterisation have been disabled in `Alcyone` to produce comparable results with `licos` and to detect the impact of the missing models.

In figure above differences on the evolution of UO2 between two different fuel models are shown. The reference radial UO2 evolution is plotted in green and the radial UO2 evolution without the HBS and transient gas swelling computation in red.

As fuel swelling is the leading phenomena for the gap closure for CMC claddings, the lack of HBS and transient gas swelling models will produce the lack of PCMI in `licos` studies with the standard gap thickness (77 μm) and CMC cladding (blue line).

The different kinetics of the expansion and the effect on the mechanical characterisation of the nuclear fuel point out that the lack of HBS modelling in `licos` will have an impact beyond the gap closure event, affecting also on the mechanical response of the cladding to PCMI.

In order to study the PCMI gap thickness will be diminished.

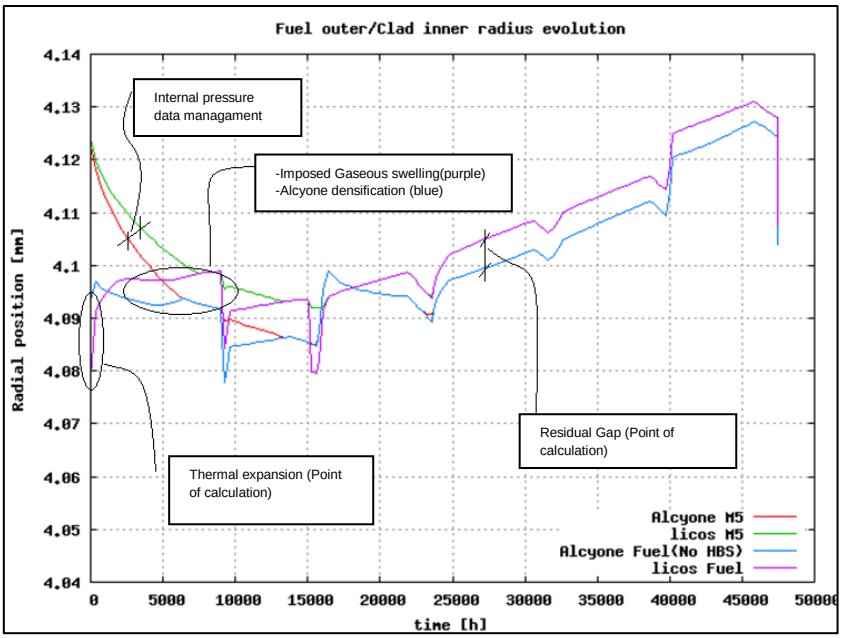


**Figure 10 Fuel-Cladding Radial Evolution**

Differences during the in-core residence in the fuel and cladding radial evolution can be observed.

Regarding the nuclear fuel, there are two main deformation phenomena implemented in `licos`, solid fission product swelling and thermal expansion.

As gaseous fission products swelling is present in `Alcyone's` computation, it has been imposed to `licos` by creating a new model which gives an approximated swelling based on the data from `Alcyone`.

Also, densification can be identified during the first cycle in `Alcyone` computation. It induces the radial decrease of the fuel (blue line) during the first 5000h.

These issues cause a difference between the two fuel radius deformation and extending it until the end of the in-core lifetime. Note that during the last four irradiation cycles, difference between radii (due to the residual gap of the different points of calculation between the two codes, cf. Annex 5) is consistent with the thermal difference observed in Figure 10.

Regarding the cladding's radial evolution, the main deformation phenomenon is creep due to the external pressure imposed by the coolant.

As observed, it is more rapid in `Alcyone` than in `licos`. This causes a small delay in the gap closure in `licos`. Some tests have been performed and it seems that the difference between the two evolutions is caused by the internal pressure. As both internal pressure evolutions are the same, the difference may be caused by how licos manages the imported data from Alcyone. Nevertheless, this conclusion is preliminary and more tests should be performed.

Despite the differences, the evolution showed is the best approach achieved by the moment.

## 3.5 Azimuthal Stress evolution

As there is not maximum admissible stress criterion available for CMCs the idea to check its viability to withstand the stresses suffered during operation is to clarify under which conditions the cladding remains under the elastic regime and, in case it is overpassed, if it remains under the failure limit.

For this purpose, the aim of the benchmark is to clarify if `licos` stress characterisation for M5 is similar to the one given by `Alcyone`, the reference code for PWR.

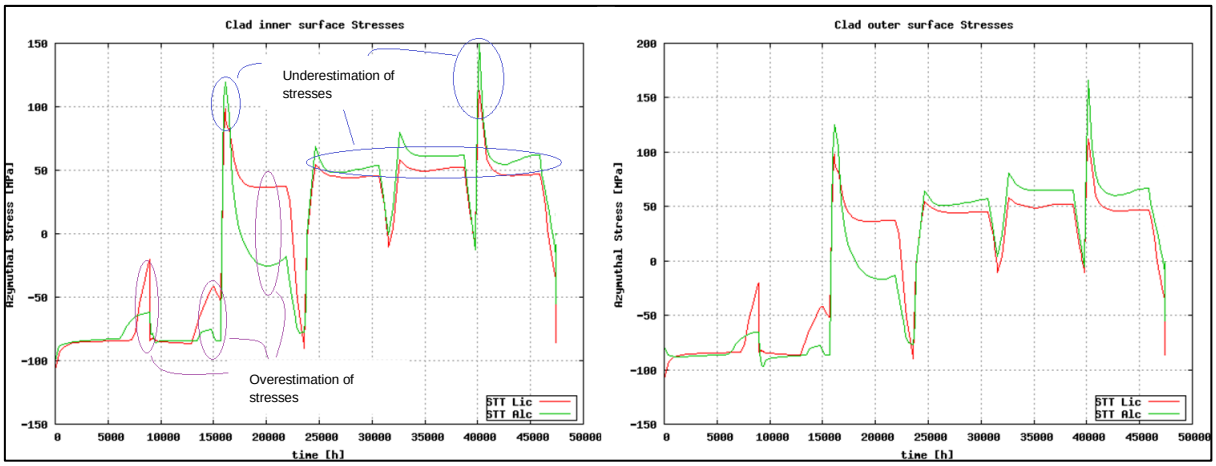


**Figure 11 Cladding Inner Surface and Cladding Outer Surface Azimuthal stress comparison**

In Figure 11 azimuthal stresses at symmetry line of `licos` computation are shown. `Alcyone` 1D calculated azimuthal stress is an average value of the stress that the cladding is suffering. Azimuthal stress is the most limiting one, being the inner and outer surface where of the cladding under more solicitations. (RENAUD, 2011, p. 30)

Few differences are observed in mechanical behaviour between `Alcyone` and `licos`.

First, at times 8000 h and 14000 h, when gap closure is achieved (cf. Figure 10) the stress calculated by `licos` is higher than the one calculated by the reference code. This may be caused by the imposed gaseous swelling in `licos`' fuel pellet. Gaseous swelling is imported as an imposed deformation over the radial direction with `Alcyone's` swelling data so it is not possible to the fuel pellet to accommodate the contact induced stress. This issue is consistent with radial evolution trend observed in Figure 10. After contact `Alcyone` fuel pellet radius tends to decrease while `licos'` one remains growing until the end of the cycle.

After the first two irradiation cycles, peak stresses calculated by `Alcyone` are higher than the ones calculated by `licos`. Also, stress relieved by fuel relocation during the third cycle is greater in `Alcyone`. This is consistent with the radial evolution shown in Figure 10.

*Summary*

Benchmarking highlights notable differences between the two codes. As expected, differences in calculation hypothesis, 1.5D vs. 2D-Rθ, and the not mature enough `licos'` fuel characterisation are source of discrepancies in the results.

The effect of the HBS in the fuel behaviour will affect directly to the mechanical response of the cladding to PCMI so the implementation of a HBS model in `licos` is highly desirable for further studies.

If fuel differences in both codes, modelling and imposed mechanical boundary conditions are taken in account; the characterisation of the PCMI by `licos` appears to be consistent with the one calculated by the reference code.

Even though the differences between two codes are evident, the computation by `licos` will allow us to have an approximate idea and an order of magnitude of the stress for the SiC-based CMC claddings.

# 4. SANDWHICH cladding

Due to the lack of characterisation of the Niobium (Nb) alloys in the plastic domain, M5 zirconium alloy has been chose for the studies of the metallic liner. Since M5 would not withstand with the high temperatures of the present SANDWHICH manufacturing process its choice has only theoretical purpose.

The choice of this material for simulations is due to its fair mechanical characterisation within the design codes and that similar visco-plastic behaviour is expected for other metallic liners.

## 4.1 Geometry's discretisation

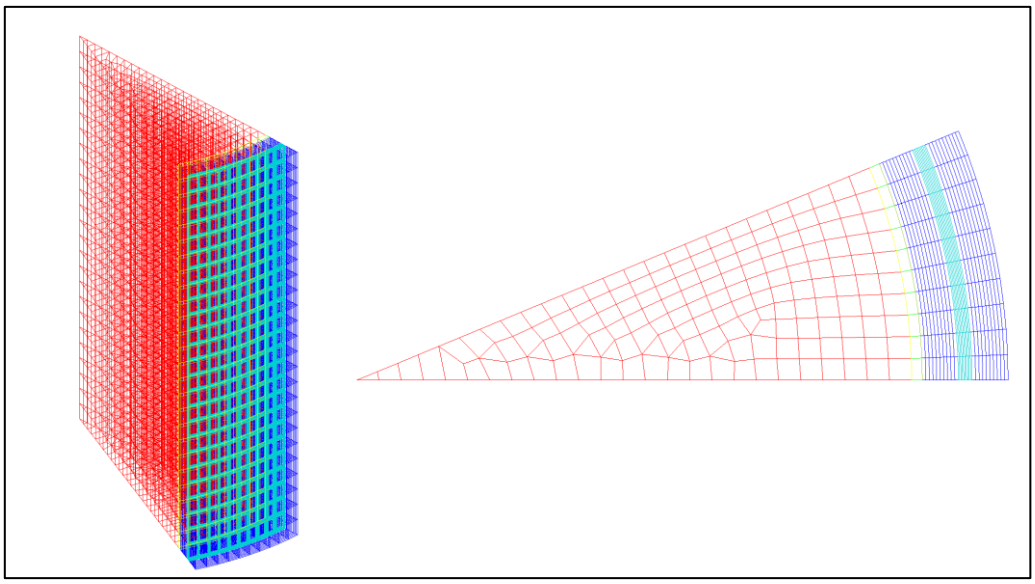

**Figure 12 SANDWICH: `licos` fuel-cladding mesh**

2D-Rθ and 3D meshes are used in `licos` simulations. For these simulations, fuel mechanical boundary conditions are those commented in 3.2.4.4.

In new simulations cladding thickness is conservative, keeping the same value as zircalloy claddings. SANDWHICH cladding has a total thickness of 625 μm.

**Table 2 Sandwich: New studies geometry**

| | Material | Thickness (μm) |
|---|---|---|
| Inner layer | $SiC_f/SiC$ | 262.5 |
| Metallic liner | M5 | 100 |
| Outer layer | $SiC_f/SiC$ | 262.5 |

$SiC_f/SiC$, the resistant part, represents 84% of the total and the metallic liner, the leak tight part, represents 14%. This is quantitatively different from TRIPLEX, where the $SiC_f/SiC$ layer represents less than the 50% of the cladding.

## 4.2 SiCf/SiC material models

SiC-CMC properties are highly dependent on their inner-structure and manufacturing process. (cf. Annex 2)
Depending on the fibre's disposition and orientation within the matrix and the fabrication process of the SiC matrix, mechanical properties may be enhanced. Figure below shows typical strain-stress curves at room temperature depending on the SiC fibres characteristics.

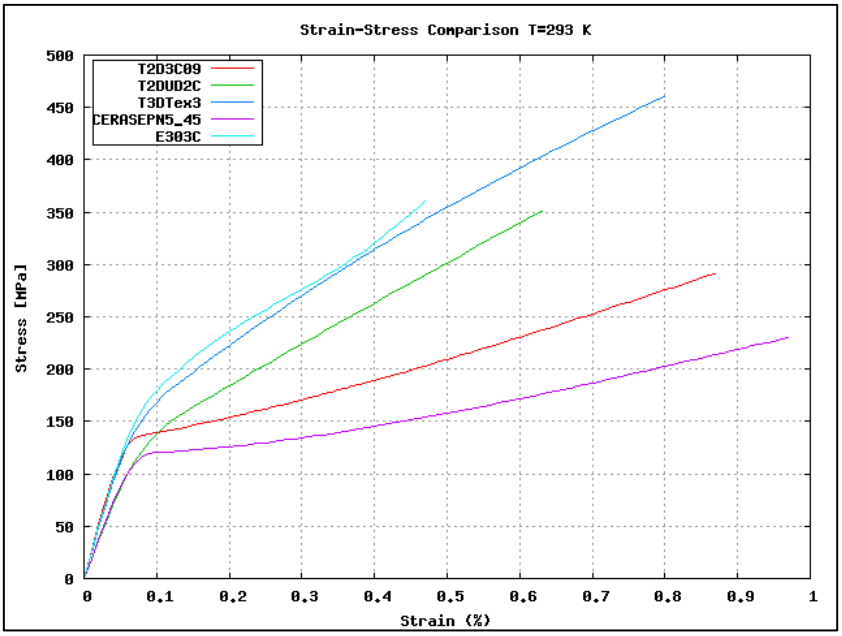


**Figure 13 $SiC_f/SiC$: Strain-Stress comparison depending on the fibres disposition.**

Table 3 below shows the resume of the mechanical properties depending on the fibre orientation. These parameters have been provided by CEA/DMN and obtained under unidirectional tensile tests with mentioned samples.

**Table 3 $SiC_f/SiC$ mechanical characteristics depending on the fibre orientation**

| Sample Reference | Geometry and layers of the sample | Pattern | Orientation (respect z axis) | Young Modulus [GPa] | Shear Modulus [GPa] | Fracture Stress [MPa] | Poisson coefficient |
|---|---|---|---|---|---|---|---|
| CERASEPN5_45 | Plane | 2D weave | 45° | $E_1$=78<br>$E_2$=$E_3$=<br>192,34 | $G_{23}$= 105,09<br>$G_{12}$=$G_{13}$=48 | 230 | $\nu_{23}$= 0.196143<br>$\nu_{12}$=$\nu_{13}$= 0.124906 |
| E303C | Cylindrical 3 layers | Filamentary wiring | 30° | $E_1$=78<br>$E_2$=$E_3$=248.11 | $G_{23}$=89.45<br>$G_{12}$=$G_{13}$=48 | 360 | $\nu_{23}$=0.159422<br>$\nu_{12}$=$\nu_{13}$=0.89256 |
| T2D3C09 | Cylindrical 3 layers | 2D braid | 45° | $E_1$=78<br>$E_2$=$E_3$=264.23 | $G_{23}$=116.41<br>$G_{12}$=$G_{13}$=48 | 290 | $\nu_{23}$=0.00736051<br>$\nu_{12}$=$\nu_{13}$=0.0039991 |
| T2DUD2C | Cylindrical 2 layers | 2D braid | Unidirectional along the layers | $E_1$=78<br>$E_2$=$E_3$=182.77 | $G_{23}$=60.03<br>$G_{12}$=$G_{13}$=48 | 350 | $\nu_{23}$=0.324282<br>$\nu_{12}$=$\nu_{13}$=0.211845 |
| T3DTex3 | Cylindrical 3 layers | 3D braid | - | $E_1$=78<br>$E_2$=$E_3$=247.07 | $G_{23}$=88.57<br>$G_{12}$=$G_{13}$=48 | 460 | $\nu_{23}$=0.0846538<br>$\nu_{12}$=$\nu_{13}$=0.0475646 |

CERASEPN5_45 will be the reference sample as it is the one used in previous studies. After that, a comparative analysis will be performed using the different samples.

## 4.3 SANDWICH Cladding under nominal conditions

For this analysis the irradiation history is the specified in 3.2.4.1. Note that in the irradiation history provided by EDF there is only one inter-cycle which reaches zero power but it will be enough to analyse the effect of the cancellation of thermal stresses in the cladding.

### 4.3.1 Radial Evolution

As mentioned in 3.4, gap closure leading phenomena with SiC claddings is fuel swelling rather than cladding's creep. Figure 14 shows the radial evolution of a monolayer $SiC_f/SiC$ cladding.

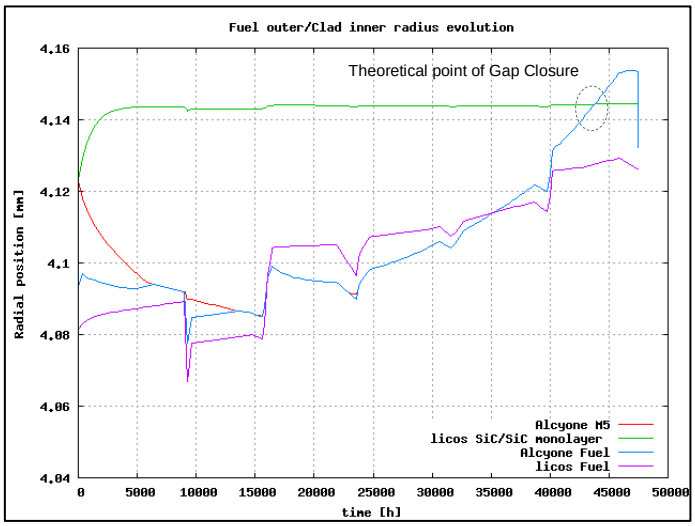


**Figure 14 UO2 Fuel & Monolayer $SiC_f/SiC$ cladding. Radial evolution with traditional gap thickness (e=77 μm).**

As mentioned in 3.4, the lack of a HBS model in `licos` fuel modelling leads to an open gap by the end of fuel rod's in-core residence time. The line in blue shows the fuel radial evolution with all `Alcyone's` physical models and the theoretical point of the gap closure.

One of the purposes of the study is to characterise the effect of the PCMI over the cladding and how the gap thickness may have a major role in keeping the PCMI under acceptable values. For this reason gap thickness is modified to force the contact.

In Figure 15 radial evolution of fuel and cladding is shown with a gap thickness of 37 μm. Contact is achieved during a nominal cycle, where the time scale of the interaction is larger and driven by the fission product swelling of the fuel pellet.

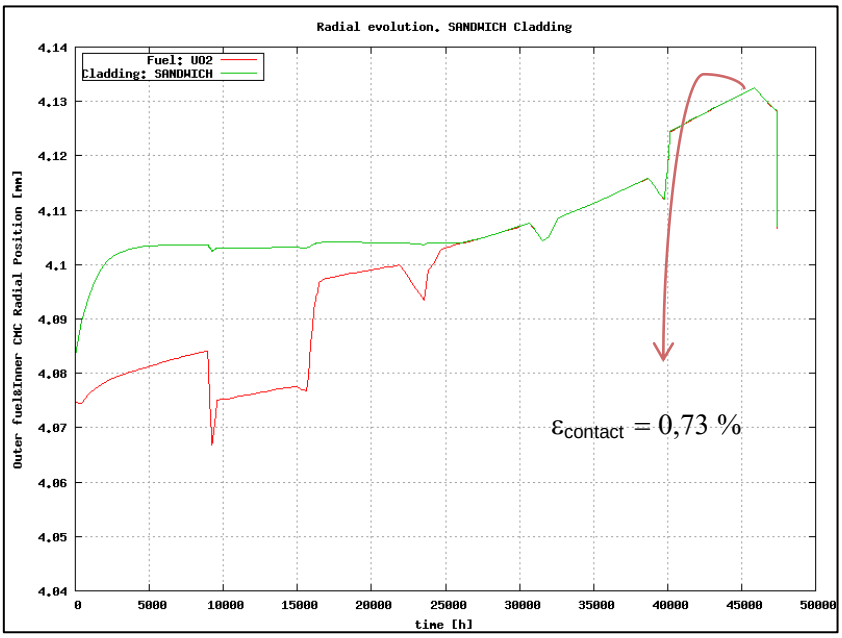


**Figure 15 UO2 Fuel & SANDWICH cladding. Radial evolution with $e_{gap}$ = 37 μm**

Interaction between SANDWICH and fuel leads to an accelerated deformation of the cladding.

The hermetic theoretical region of $SiC_f/SiC$, up to 0,04% (when micro-cracking begins), has been overpassed due to strain imposed by fuel's expansion, up to 0.73% by the end of in core residence.

As `licos` simulation is not realistic, at this point the only conclusion that can be made is that the imposed deformation by fuel's expansion may reach unacceptable strains for SiC-based CMCs. If PCMI is supported, gap thickness will play a major role in the limitation of the in-core residence time.

### 4.3.2 Thermal Evolution

Due to the low thermal conductivity of $SiC_f/SiC$ (cf. Annex 2.1.4) and the multi-layered structure, temperatures across the cladding and fuel pellet are increased.

The thermal gradient across the cladding is source of thermal stresses in each layer of the cladding due to differential thermal stresses and between the metallic liner and the $SiC_f$/SiC layers due to the different thermal strain coefficient (cf. Annex 7)

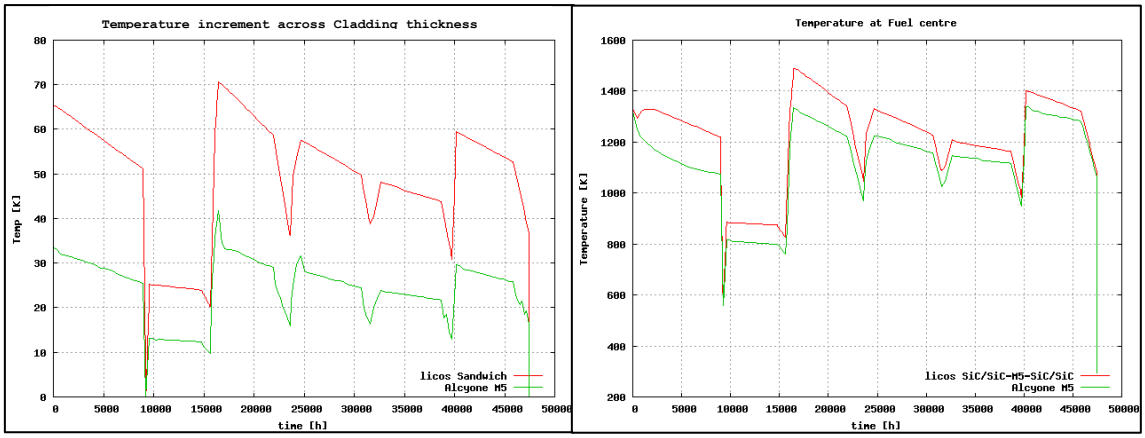


**Figure 16 SANDWICH: Thermal Increment across cladding thickness & Fuel Centre Temperature**

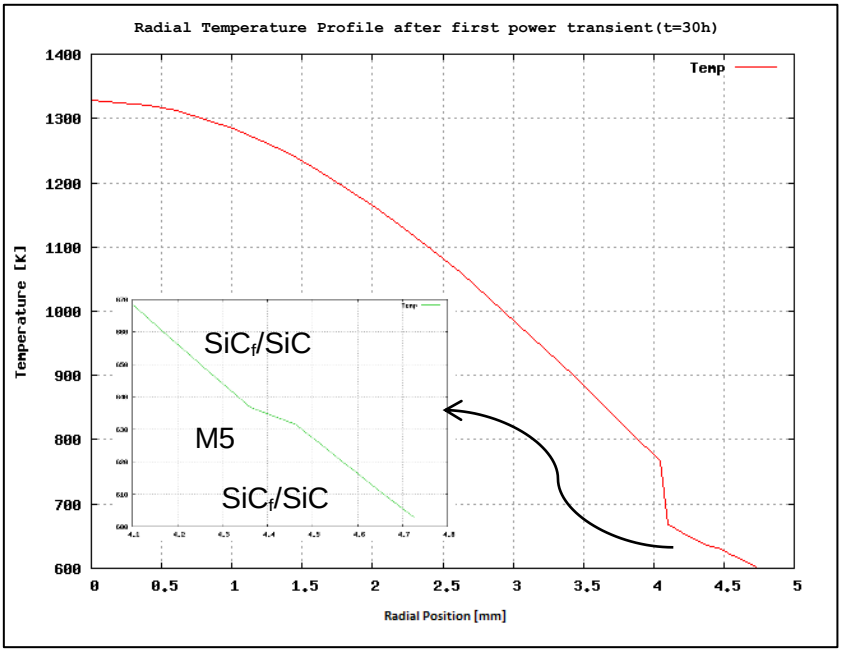


**Figure 17 SANDWICH: Radial Temperature Profile after first power transient ($T_{max}$)**

In Figures 16 and 17, the impact of the low conductivity of the Sandwich cladding is shown.

As can be observed, the thermal differences between the internal and external cladding surfaces are increased, which will induce more thermal stresses.

Also, fuel pellet temperature is increased. This reduces the safety margin for fuel melting.

### 4.3.3 Stress evolution

In Figure 18 Von Mises equivalent stress shows the location of stress concentration in the cladding. It represents the state of stress after contact between fuel and cladding.

As can be observed, there is a ‘hot spot’ at the fuel fracture plane. Stress concentration factor is 1.3 approximately but it may vary depending on the contact condition.

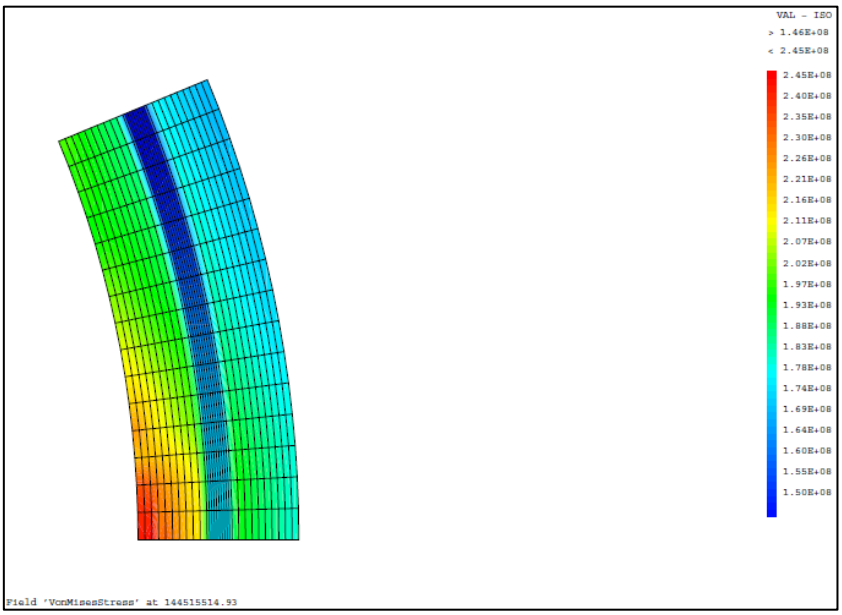


**Figure 18 Stress concentration at $\theta = 0$: Fuel fracture plane.**

In Figure 19 and Figure 20 azimuthal stresses at points of interest of the cladding are shown.

The two images correspond to the different boundary fuel planes. 2D-R$\theta$ computation permits to detect 'hot spots' where tensions are concentrated. In case of contact, due to the friction between fuel’s external face and the first cladding layer’s inner surface, tensions are concentrated at the fuel fracture plane. (cf. Figure 18)

Figure 19 and Figure 20 shows at first sight that under nominal conditions and until gap closure, the liner and the outer CMC layer remain under compression but not the inner layer. Irradiation induced swelling drives the inner cladding into a tensional state while the remaining layers remain in a compression.

Previous studies revealed that the ceramic layers remained under compression during the first irradiation cycle. After CMC swelling, metallic liner suffered tensions in excess which suggested that the metallic layer may be work under visco-plastic regime. (RENAUD, 2011)
The transition in actual simulations from compression to tension is due to the updated SiC swelling law. It had a lower saturation value in the preliminary analysis so the induced deformation, and thus the suffered stress, was being underestimated. The effect of metallic creep also is taken into account and is explained with more details in 4.3.3.1.

Although the inner layer is under tension, it remains under the elastic limit of the SiC-based CMC.

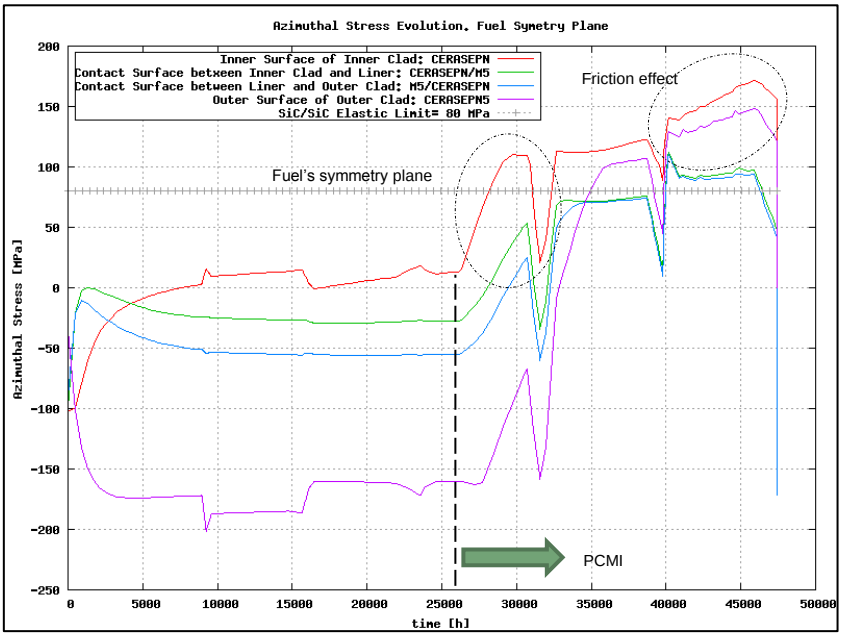


**Figure 19 Azimuthal stress evolution during in-core residence at Fuel symmetry plane.**

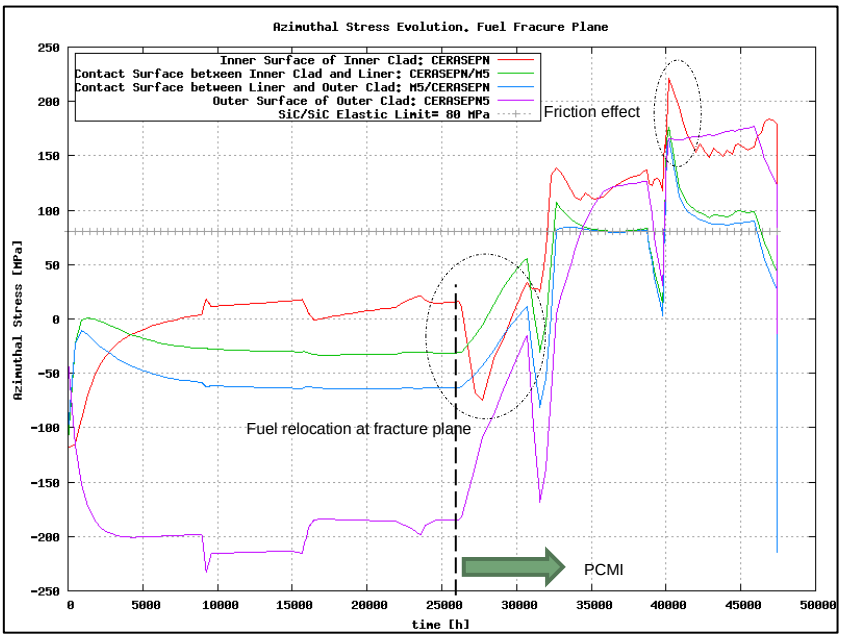


**Figure 20 Azimuthal stress evolutions during in-core residence at Fuel's fracture plane**

After PCMI, induced stresses depend on the type of interaction between the fuel and the cladding. This is explained with more details at 4.3.3.2

#### *4.3.3.1 Thermal transient and swelling induced stresses: First irradiation cycle and inter-cycle*

One of the primary interests of these studies is to analyse the mechanical behaviour of the SANDWICH cladding during power transients and due to swelling taking in account the metallic creep and plasticity.

As thermal stresses appear following the power rise, they are not susceptible to be relaxed in a short term. This fast deformation kinetics cause the compression of the metallic liner, as it tends to expand more than the ceramic layers.

In Figure 21 differences in the azimuthal stress evolution due to the consideration of the plastic deformation of the metallic liner are shown.

Results are consistent with previous studies but with a lower tensional state for the liner at the end of the cycle due the different metallic materials, M5 zirconium alloy instead of Nb alloy. (cf. Annex 7)

Considering the elastic model, after the power transient $SiC_f/SiC$ irradiation induced swelling is driving the metallic liner to a traction tensional state (green and blue lines).

Note that the azimuthal tension of inner surface of the inner CMC layer (red line) is barely evolving during the irradiation cycle.

Some tests point out to the liner as responsible of this evolution but it remains an open question how the liner can drive the inner layer stress evolution by compensating the swelling induced stresses.

Considering the visco-plastic model, in image at right, creep mechanisms are relieving metallic liner tensions, maintaining the metallic liner under compression and leading the inner layer into tension.

At t=9000 h power is off and the thermal gradient across the cladding is cancelled and thus thermal stresses.

As can be observed, thermal stresses compensated part of the swelling induced stresses, inducing a peak stress when they disappear. Nevertheless, the peak suffered by its cancellation appears to be less important than the initially expected.

Differential swelling stresses compensates the differential thermal stresses, so the cancellation of the thermal gradient, and thus the thermal stresses, should lead to a stress greater than the observed, in the order of 50 MPa. (cf. Figure 23)

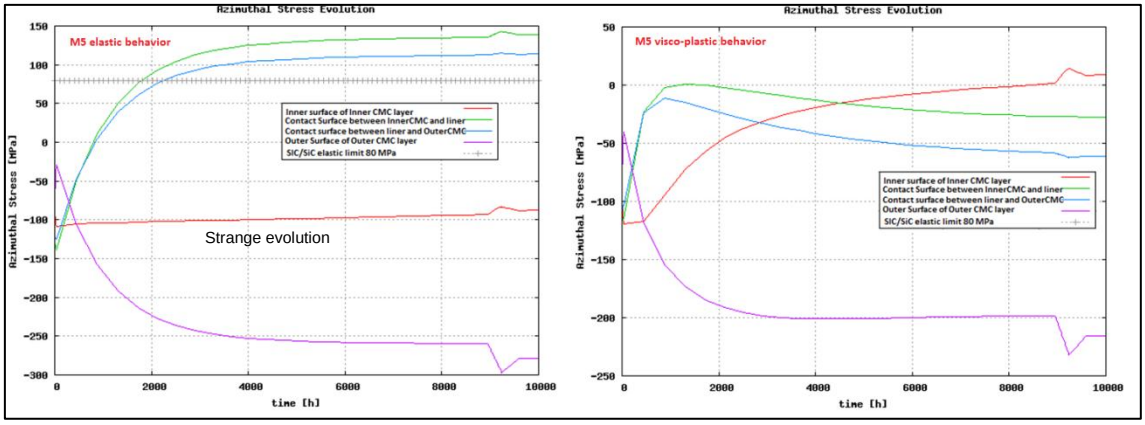


**Figure 21 SANDWICH: Azimuthal Stress evolution during the first irradiation cycle. Visco-plastic vs. elastic effects**

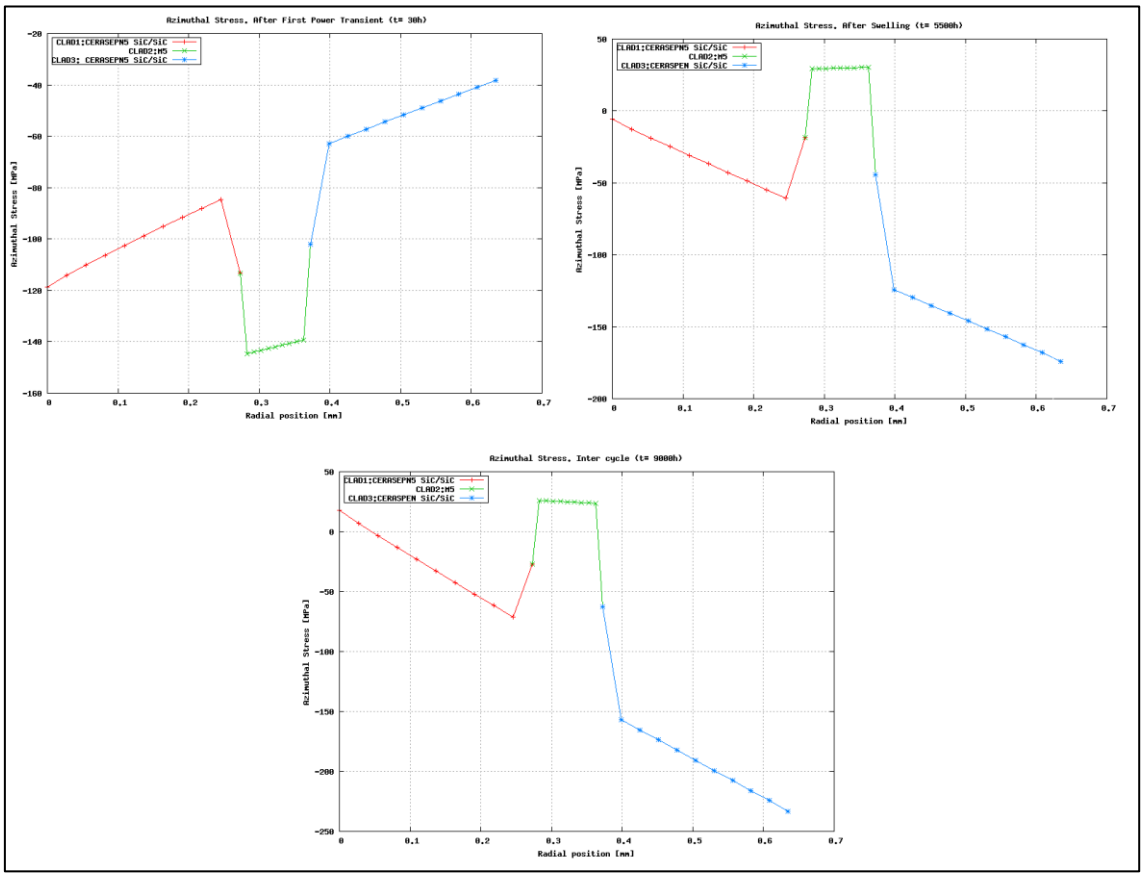


**Figure 22 SANDWICH: Azimuthal stresses. Radial plots: After first power transient, after swelling and Inter-cycle.**

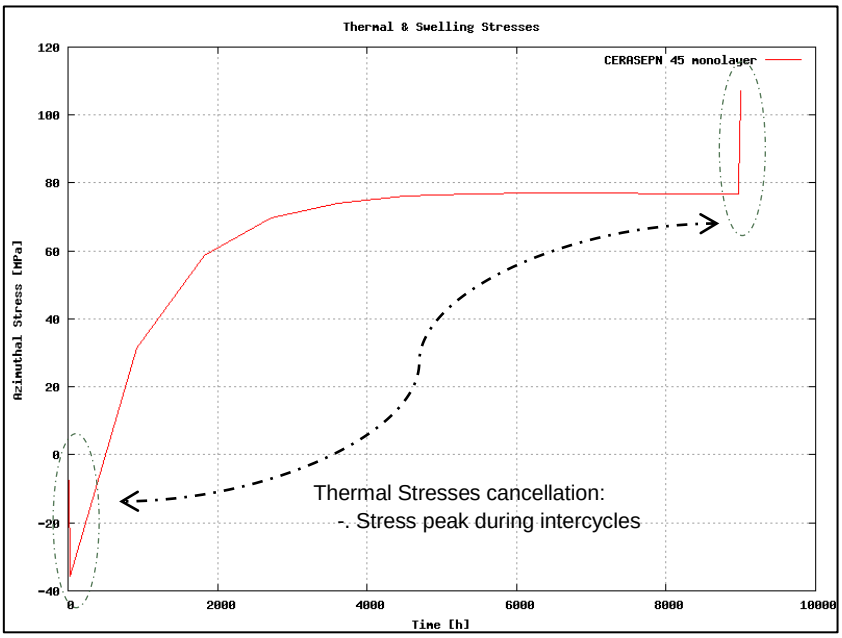


**Figure 23 Monolayer SiCf/SiC: Thermal and Irradiation Induced Swelling Stresses**

The fact that the CMC layers remain under compression implies not only the risk of

cracking induced failure is minimized but also its leak-tightness is increased during this stage. This is an effect of the closure of thermal micro-cracks and porosity introduced during processing.

Also, tensional state of the metallic liner is better characterised as it takes in account the stress relaxation by plastic deformation. The level of stress is below the elastic limit of $SiC_f$/SiC and thus it may be acceptable.

In conclusion, *Sandwich* cladding under nominal power rise and shutdown without PCMI may keep its integrity and leak-tightness, nevertheless uncertainties linked to the `licos` simulation must be clarified.

#### *4.3.3.2 Pellet-Cladding Mechanical Interaction*

At t≈26000 h PCMI is achieved. As seen in Figure 15, strain caused by pellet cladding contact is driven by fission products swelling during nominal operation and by thermal expansion during inter-cycles.

During the first part of the contact, the slow kinetics of the interaction allows stress relaxation by fuel creep. PCMI have different impact over the inner layer of the cladding depending on the position. At fuel's symmetry plane contact increases cladding tension while at the fracture plane, as the fuel boundary allows negative displacements reducing the impact (cf. 3.2.4.4), compression takes place to compensate the induced stress. Also, this partially compensates swelling induced stress at this point. (cf. Figure 19 and Figure 20).

Under PCMI condition, nominal power transients may be critical. As can be observed, fast kinetics of fuel's thermal expansion produce a stress peak as the fuel is not able to creep in short scale. This effect is more accentuated at fuel's fracture plane due to the friction between fuel and cladding.

This tension peak, added to the accumulative strain induced by the fission products, drives the cladding over the theoretical elastic limit, 80 MPa, since the first inter-cycle after contact. Beyond this point, SiC based CMC loses its hermeticity.

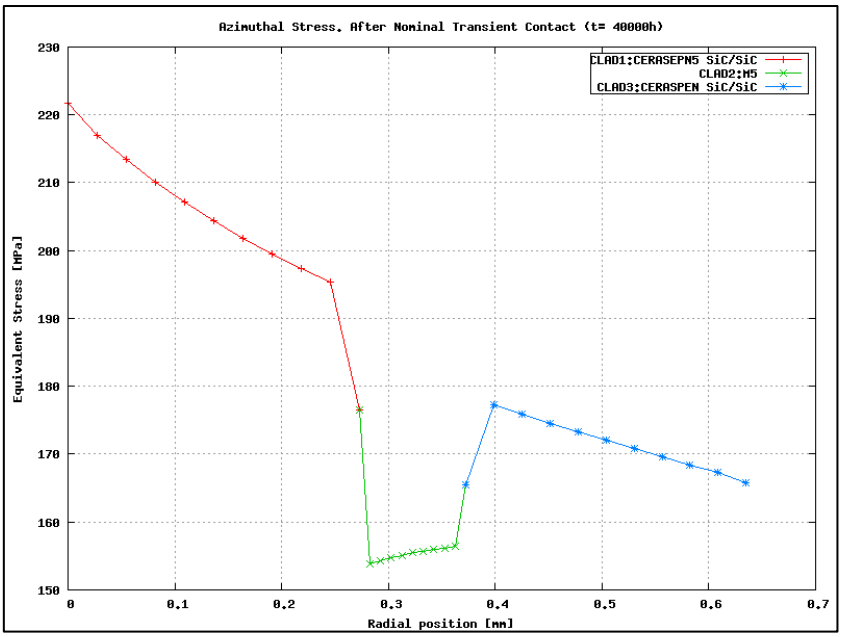


**Figure 24 SANDWICH: Radial azimuthal stress under PCMI (θ=0º,t=40000 h)**

Figure 24 shows the radial profile of azimuthal stress at t=40000 h, just after the last power transient.

Even though the $SiC_f/SiC$ inner layer is near the fracture limit (CERASEPN 45 $\sigma_f$=230 MPa), the stress suffered by the liner is not too excessive and may make possible to keep leak-tightness even at this conditions.

#### *4.3.3.3 SiC-based CMC comparison*

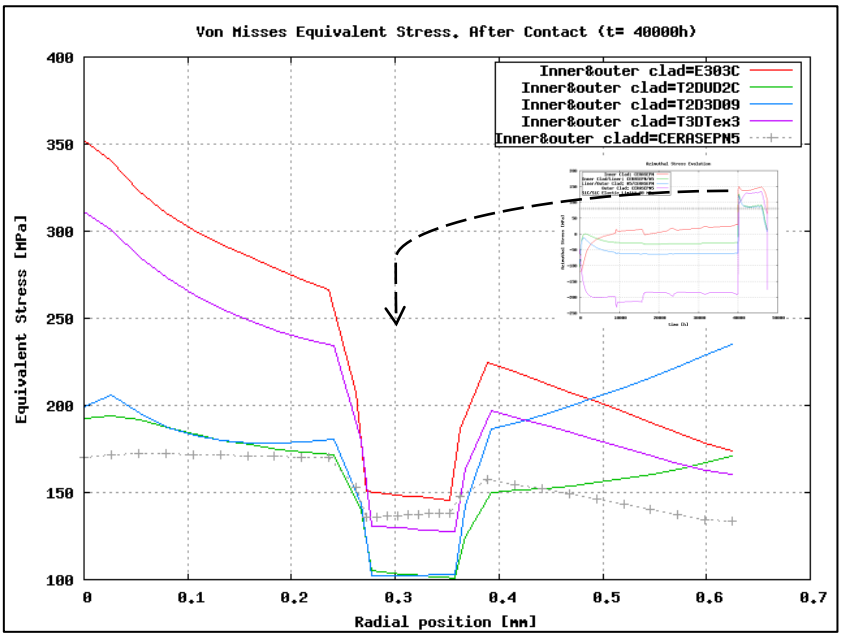


**Figure 25 Von Mises stresses after PCMI for different $SiC_f/SiC$ types.**

Figure 25 shows the different response to the violent interaction between fuel and cladding during a power transient. As can be observed, independently of the type of $SiC_f/SiC$, the inner layer of the cladding is near the failure limit.

For compatibility reasons between fuel and cladding, inner cladding is meant to be made with SiC fibres disposed with filamentary winding SiC fibres.

As both ceramic layers, inner and outer, have lost their hermeticity at this point, the selection criteria to the outer layer will be to minimize the impact over the metallic liner, as it's the layer which keeps the leak-tightness.

Reference design for accidental scenarios will consist in an inner filamentary winding and outer 2D-45º braid $SiC_f$/SiC layers.

## 4.4 $SiC_f$/SiC Cladding under accidental conditions

Once that SANDWICH cladding response has been characterized under nominal conditions (cf. 4.3.3) next step is to characterize its response to accidental power transients.

The fast evolution of the fuel power produces a sudden increase of temperature on the cladding.

Transient power with a ratio of 88 W/cm·min$^{-1}$ has been used to simulate the accidental scenario. This power kinetics are extremely fast in comparison with nominal power transients, in the order of 0,13 W/cm·min$^{-1}$, and may produce violent response of the materials dealing to failure.

Irradiation history used in previous studies has been modified by triggering the accidental power ramp in three different cases in different fuel pellet-cladding relative positions.

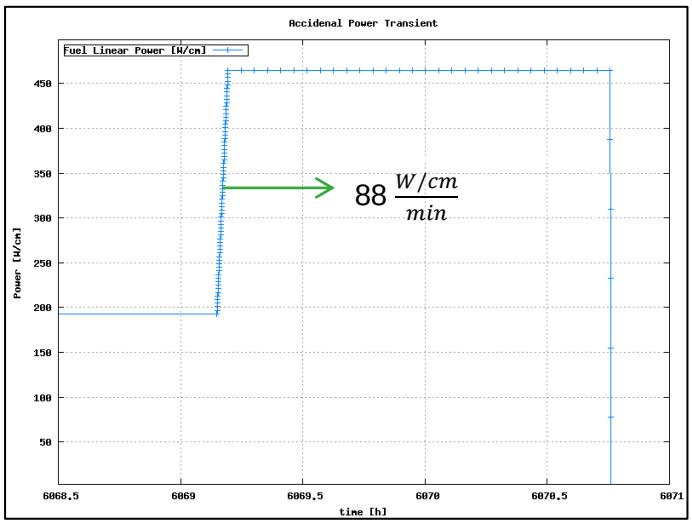


Figure 26 RIA power transient

### 4.4.1 Fuel-Cladding response

#### *4.4.1.1 Without gap closure*

Thermal expansion of the fuel pellet does not lead to contact situation.

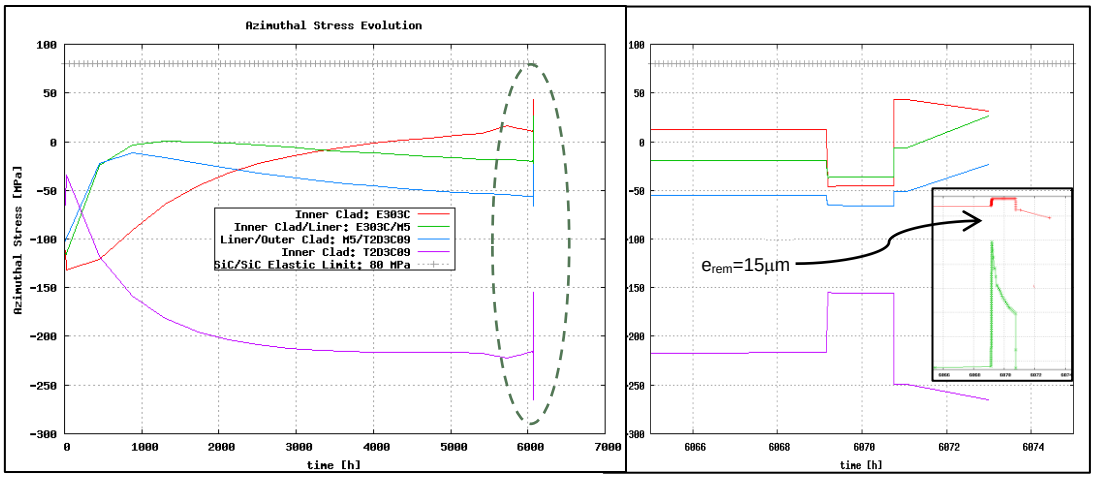


**Figure 27 Accidental Power transient. Azimuthal Stress and Radial evolutions. No gap closure.**

Thermal gradient during the transient induces thermal differential stresses which counteract the swelling induced stresses. Once the power is set off, cancellation of thermal gradient restores the induced swelling stresses.

As can be observed, stresses do not overpass the elastic limit of the ceramic layers in this accident situation. (cf. Figure 27)

#### *4.4.1.2 With gap closure*

In this situation, thermal expansion of the fuel pellet produces the contact between the inner layer and the UO2.

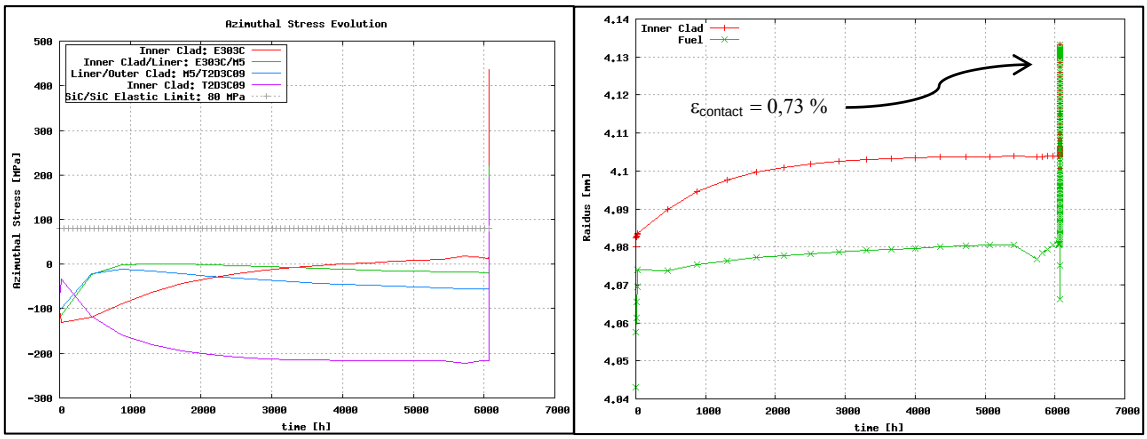


**Figure 28 Accidental Power transient. Azimuthal Stress and Radial evolutions. Gap closure.**

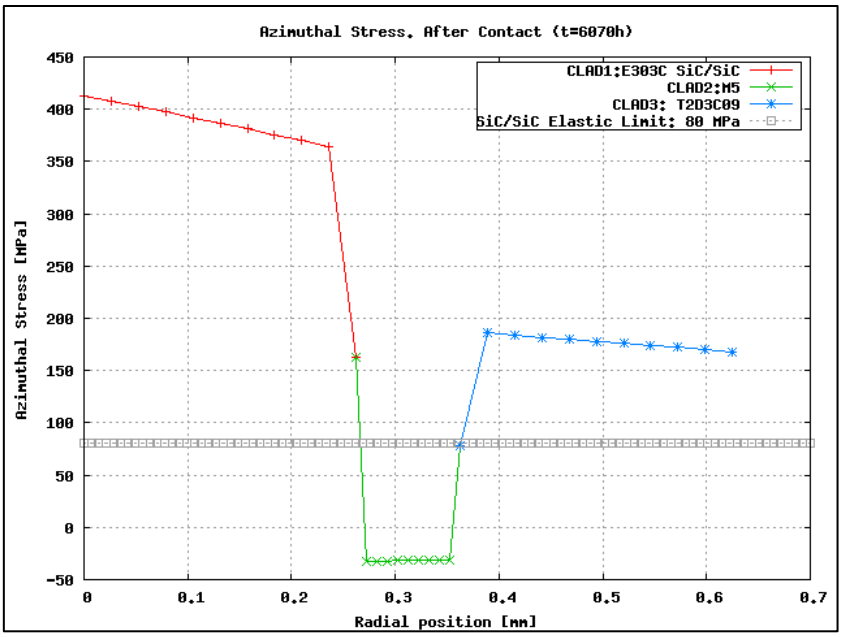


Figure 29 Accidental power transient. Azimuthal Stress radial profile. Gap Closure.

The rapid kinetics of the contact produces a strong interaction between fuel and Inner cladding.

PCMI overpasses fracture limit of ceramic layers (cf. Table 3). As can be observed in Figure 29, difference of thermal expansion kinetics induces compression into the metallic liner.

Even though the ceramic layers have lost their integrity the metallic liner remains under compression. This would mean that integrity of the liner would keep the hermeticity of the cladding.

#### 4.4.1.3 *Fuel-Cladding response with previous contact*

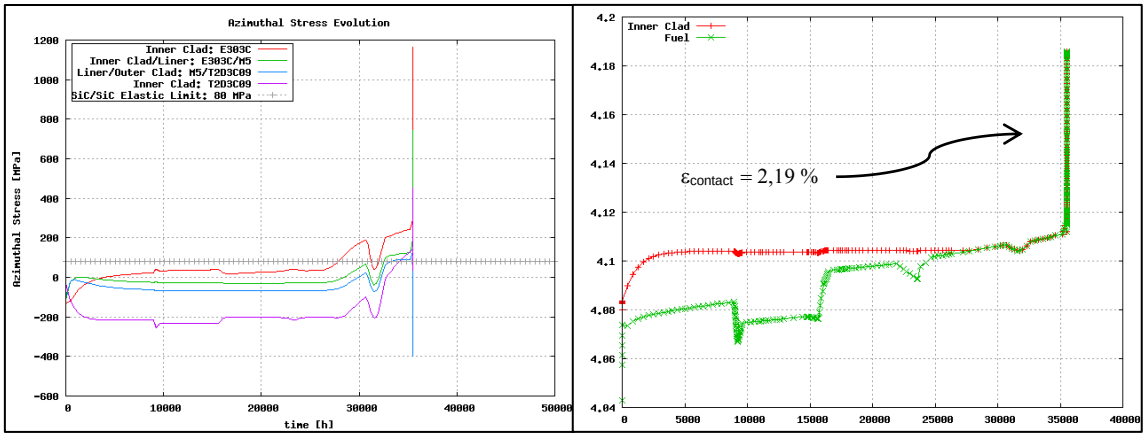


Figure 30 Accidental Power transient. Stress and Radial evolutions. Previous PCMI.

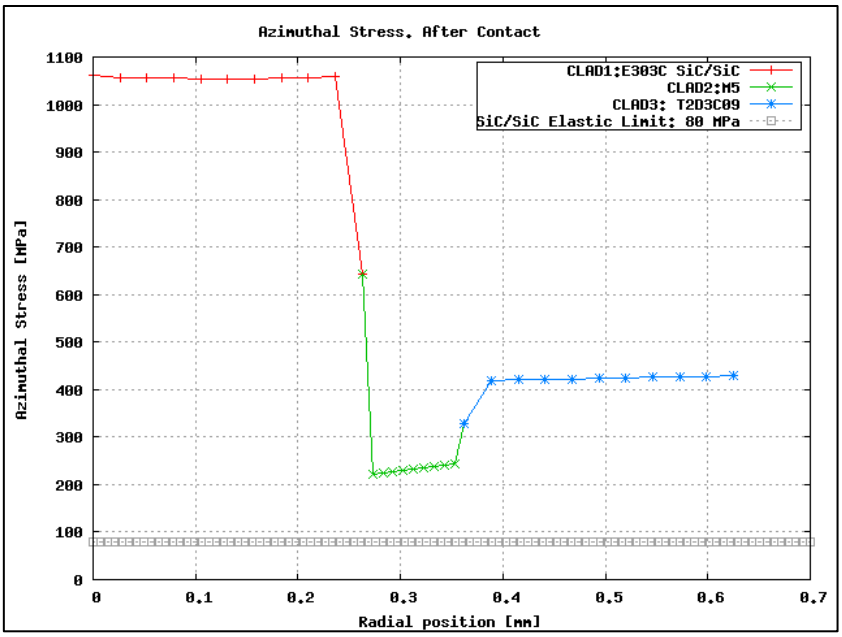


**Figure 31 Accidental power transient. Azimuthal Stress radial profile. Previous PCMI.**

Previous PCMI enhances the destructive effect of the violent interaction due to the fuel's thermal expansion as the cumulated value of strain doubles the theoretical range of integrity.

Nevertheless, uncertainties about the contact characterization between ceramic layers and liner do exist as the impact of the ceramic rupture over the metallic layer is not taken into account and it may induce damage.

No assumptions of the response of the cladding may be done under strong PCMI.

# 5. Summary, Conclusions & Future perspectives

New SiC-based cladding designs have been proposed as a replacement of zirconium alloys tubes for LWRs' current claddings.

Two are the most studied designs: American *Triplex*, a fully SiC-based ceramic cladding, and CEA's *Sandwich*, a SiC-based CMC cladding with a metallic liner.

*Sandwich* design aims to solve some of the drawbacks of the Triplex design, such as the potential lack of hermeticity and the end-cap bonding problem.

Even though many efforts have been dedicated to the test the *Triplex* behaviour under PWR conditions, thermo-mechanical and PCMI *Triplex* response are poorly characterised.

Regarding *Sandwich, CEA's* characterisation of the multi-layered cladding is devoted to analyse the impact caused by in-core operation under PWR conditions, emphasizing on the thermal and PCMI effect over the cladding, with the aid of design codes for advanced thermo-mechanical studies.

## 5.1. Conclusions.

Previous studies characterised the behaviour of the multi-layered cladding under PWR nominal conditions. Although these studies are very preliminary, they showed encouraging results.

The aim of this study is to provide further information about the *Sandwich* response by emphasizing its characterisation in power transients and to study the effect of the PCMI in the cladding.

In order to have more detailed studies one reference case for an under-development design code which allows working with non-standard geometries, `licos`, has been created.

To verify the validity of the results and to detect uncertainties and its limitations benchmarking against the CEA's PWR reference code, `Alcyone`.

### 5.1.1. Thermo-mechanical Analysis

Nominal and accidental power transients have been characterised considering the effect of the contact between the fuel pellet and the cladding.

#### *5.1.1.1. Open Fuel-Cladding Gap*

Sandwich response to in-core solicitations during nominal conditions appears to be consistent with previous studies but with some particularities.

During the first power transient, the apparitions of differential thermal gradient drive the cladding into compression due to their different thermal expansion coefficients. Also the differential thermal stresses drive the inner CMC layer to compression and the outer layer to tension state.

Nevertheless, during the first irradiation cycle, irradiation induced swelling appears and compensates thermal stresses and forces the metallic liner into tension. Once irradiation swelling is saturated, metallic creep compensates the secondary stresses.

During the inter-cycle, thermal stresses cancellation are supposed to cause a peak of stress in the ceramic layers. Although this increment of the stress is observed, the obtained results appear to be less than the expected.

During accidental transients, the sudden apparition of a big thermal gradient across the cladding enhances the thermal stresses.

During the power rise this stresses compensate the induced swelling stresses driving the ceramic layers to compression. Once that the accidental transient is finished and the fuel power is off, the restoration of the swelling induced stresses induce a peak of tension.

The ensemble of the cladding remains under the elastic limit of the SiC-based ceramic layers so it may be possible to the Sandwich cladding to withstand this type of scenario.

#### *5.1.1.2. Closed Fuel-Cladding Gap*

Interaction between fuel pellet and cladding is of special interest as it may cause the cladding failure.

If PCMI is achieved during nominal operation, the slow kinetics of the contact allows stress relaxation by fuel creep. Nevertheless, during transients, nominal and accidental, the stresses suffered by the inner ceramic layer are under unacceptable values for the SiC-based composite.

Also, the effect of the ceramic layer damage over the metallic liner is unclear, so it is not possible to assure that the metallic liner will keep its integrity under these conditions.

In conclusion, gap resizing will play a major role in the fuel rod design to increase its in-core lifetime.

### 5.1.2. Limitations and uncertainties

Licos benchmarking pointed out many limitations, mainly in the fuel modelling.

The lack of a HBS and gaseous swelling models for the UO2 fuel has direct consequences on the estimation of the gap closure. Also, as fuel expansion kinetics will be affected, the interaction between fuel and cladding is subjected to uncertainties.

The lack of a thermo-hydraulic model forces us to import data from the reference code also introducing uncertainties.

Regarding the mechanical modelling, the bonding between the metallic layer and the ceramic does not represent the possible interaction under strong loads.

## 5.2. Suggested future work

In comparison to *Triplex, Sandwich* appears to maintain its leak-tightness even when the ceramic layers are not working under compression thanks to the metallic liner.

Further studies should be addressed to minimize the uncertainties around the thermo-mechanical characterisation.

By the moment, a thermo-hydraulic model should be implemented. This would allow having full multi-layered fuel rod simulations. Also, enhanced material models should be implemented, especially those regarding the fuel volumetric evolution and mechanic characteristics as HBS formation and gaseous swelling.

Also, the mechanical characterisation of the contact between layers should be enhanced to allow a better understanding of the strong PCMI as the ability of *Sandwich* to withstand this situation is still not clear.

In conclusion, *Sandwich* studies are still in a preliminary stage but with encouraging perspectives.

## Bibliography


1. Feinroth, H., & Hao, B. (2006). *Patent No. US 2006/0039524 A1.* USA.
2. HELFER, T. (April 2012). *Notice de Presentation de l' application* `LICOS` *v 1.0.* CEA/DEN/CAD/DEC/SESC/LSC NT-0.
3. Katoh, Y., L.L., S., Henager Jr, C., Hasegawa, A., Kohyama, A., Riccardi, B., et al. (2007). Current Status and critical issues for development of SiC composites for fusion applications. *Journal of Nuclear Materials*.
4. Kazimi, F. (2011). *Feasibility and Economic benefits of PWR Cores with SiC cladding.* MIT-ANP-PR-134.
5. Lahoda, E., Johnson, S., & Ray, S. (2011). *Challenges in the Development of Silicon Carbide Advanced Fuel Cladding for LWR application.* Westinghouse Electric Company.
6. MARELLE, V. (02/2012). `ALCYONE` *V1.2.3: Notice de presentation.* CEA/DEN/DEC/SESC/LSC NT 12-002-ind 0.
7. Meteor V2. (2006). *SESC/LSC ind 0 juin 2006.*
8. Nuclear Energy Agency. (2009). OECD.
9. Pelletier. (2010). *Concept du crayon REP à gaine céramique. Première evaluation du comportement.* CEA/DEN/CAD/SESC/LSC NT 10-043-Ind 0.
10. RENAUD, C. (2011). *Analyse du comportement thermomechanique d' un element combustible a gainage multicouche, dans le cadre d' une eutd de predimensionnement pour la filiere REP.* CEA.
11. Stempien, J., Carpenter, D., Kohse, G., & Kazimi, M. (2011). *Behaviour of Triplex SiC Fuel Cladding Designs Tested Under Simulated PWR Conditions.* MIT-ANP-TR-135.
12. ZABIEGO, M. (2011). *Data for the GFR pin design.* CEA/DEN/CAD/DEC/SESC 11-006-Ind. 0.
13. Zabiego, M. (2011). *Gainage a base SiC pour les REL.* CEA/DEN/CAD/DEC/SESC/LC2I.

# Annex 1

## Zirconium Alloys: Damage

Damage suffered throughout nominal reactor operation exposure limits the in-core residence time (Nuclear Energy Agency, 2009,pg.55-64 ):

- Uniform waterside corrosion. Cladding oxide thickness, with burn-up in excess of 50 GWd/t, can exceed 100 µm. This oxide layer induces cladding hydriding as 15 to 20% of the hydrogen generated by corrosion is absorbed into the zirconium alloy.
- Hydriding induces embrittlement of the cladding over 2000 ppm hydrogen overall concentration at operation temperature. It also affects cladding ductility at lower temperatures when hydrogen concentration is around 600-800 ppm.
- Radiation induced structural damage induces an increase in the yield stress as the ultimate strain decreases.
- Creep: Ballooning of the fuel rod may block the coolant flow channels over heating the zone.

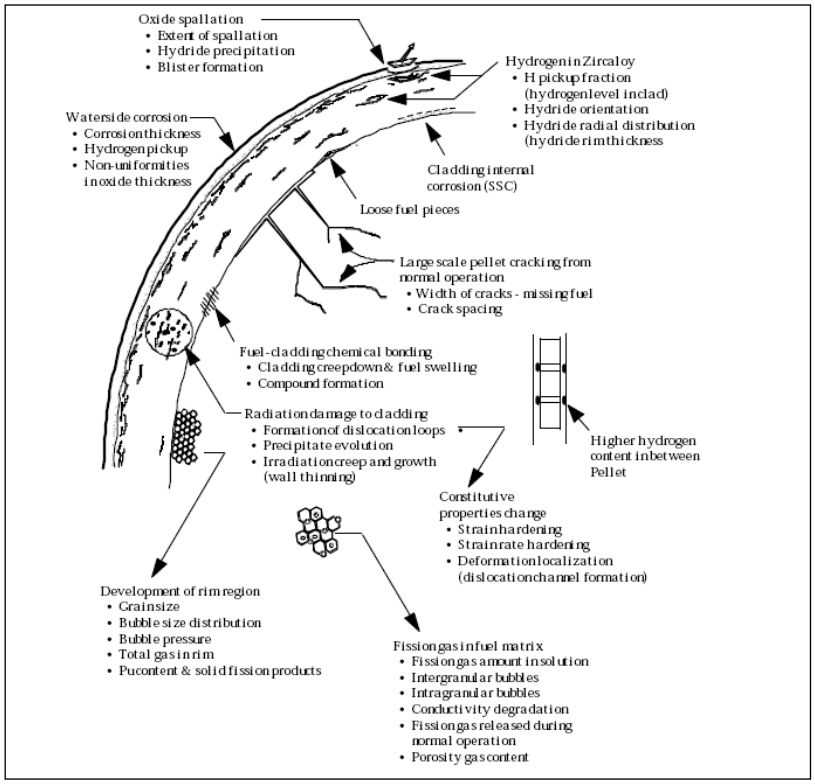


**Figure 32. PWR fuel/cladding state at high Burn-Up**

Despite of the improvements achieved by the different generations of zirconium alloys, hydrogen embrittlement and high exothermic oxidation reaction over 1000°C increases their vulnerability during accidental transients.

# Annex 2

## Silicon Carbide Ceramic Composites Properties

### 1. SiC and SiC-based composites: Strengths and weaknesses.

Silicon carbide (SiC) is the non-oxide ceramic material considered for industry applications for its hardness and corrosion resistance at high temperatures. Regarding the nuclear industry, the high thermal conductivity and low thermal expansion coefficient (which may allow achieving higher linear power rates with lower thermal stresses) the neutron transparency and the after irradiation low rates make this material a matter of interest.

Up to now, SiC has been used as a barrier layer for coated fuel particles in gas-cooled reactors and also in aeronautical and high temperatures environments, as gas turbines. Also it is intended to be used in nuclear fusion applications and advanced fission reactors.

#### *1.1 Monolithic SiC*

SiC various properties may be attributed to its crystal structure. The most common are α-SiC, rhombohedral and hexagonal polytypes (Ramsdell notation[4]: 4H, 5H, 15R) and β-SiC, with cubic crystal structure (Ramsdell notation: 3C) where β-SiC is the more stable phase at temperatures below 2000ºC where undergoes through a phase change to α-SiC.

Due its crystallinity, SiC is susceptible to brittle fracture. Brittle fracture is a process by which cracks form and propagate through a cross section of the material in a direction perpendicular to the direction of the imposed load. For plastic deformation, dislocation in the crystal structure must be able to diffuse in response to the applied stress. SiC crystal structures have few slip systems making difficult the dislocation motion. (Stempien, Carpenter, Kohse, & Kazimi, 2011)

**Table 4.** Typical values of different cladding materials' properties (Lahoda, Johnson, & Ray, 2011)

| Material | Tm(°C) | $\sigma_c$ (barns) | K (W/m/K) | Hardness (HVN) | E (GPa) | $K_{Ic}$ (MPa·m$^{0.5}$) |
|---|---|---|---|---|---|---|
| **Zr alloys** | 1852 | 0.185 | 16 | 300 | 99 | 90 |
| **Non irradiated monolithic SiC** | 2545 | 0.175 | 80 | 2800 | 380 | 4 |

As a semiconductor, SiC has a low density of valence band electrons which means that heat diffusion is mainly due to the travel of vibrational lattice waves (phonons). Thermal diffusivity rapidly decreases with the irradiation damage induced into the crystalline structure. (Stempien, Carpenter, Kohse, & Kazimi, 2011) This is a potentially limiting property as regards fuel cladding applications.

[4] In Ramsdell notation first number denotes the number of Si and C bilayers(bA, cA, aB, cB, aC and bC) followed by a letter, C, H or R depending de crystal symmetry (cubic, hexagonal or rhombohedral)

### 1.2 $SiC_f/SiC$

SiC-based CMC is formed basically of three components:

1. SiC fibers (diameter<20 µm) representing 30-40% of the composite.
2. Interphase material which covers every fiber (i.e. PyC)
3. SiC matrix

This SiC composite responds to the mechanical drawbacks of monolithic SiC. Despite of being ceramic, this composite has a pseudo-ductile behavior (strain of 1%) at macroscopeak scale which confers a graceful failure mode, being the composite's fracture toughness on the order of 20 $MPa \cdot m^{0.5}$ (Lahoda, Johnson, & Ray, 2011).

### 1.3 $SiC_f/SiC$ pseudo ductile behavior

Pseudo-ductility in ceramic composite materials is directly related to mechanisms that progressively damages the composite. Micro-crack formation and propagation across the SiC matrix is limited by the SiC fibers. Matrix cracks propagate due to the time-dependent elongation of crack-bridging fibers because fibers carry the highest stresses as they bridge across the crack. For composites where matrix creep can be ignored, matrix crack grows through fiber creep processes. (Katoh, et al., 2007)

### 1.4 Thermal conductivity

Thermal conductivity of non-irradiated CMC is dependent of the used materials and manufacturing processes. The different weaving of the fibers, 2D or 3D, and the matrix residual porosity (10-20%) has a significant role in this property. SiC based composites' thermal conductivity (10-50 W/K/m) is significantly inferior to the monolithic SiC (65-200 W/K/m). (Katoh, et al., 2007)

### 1.5 Hermetic behavior

Hermeticity is a major issue for applications that require a pressure boundary and gas containment. The matrix micro cracks, existing more or less in the as-fabricated and damaged $SiC_f$/SiC, cause potentially gaseous fission products release in case of LWR use.

**Table 5 Properties for SiC/SiC and typeakal values for CVI and NITE composites. Adapted from (Katoh, et al., 2007)**

| | | | FCI | 2D CVI | 3D CVI | NITE |
|---|---|---|---|---|---|---|
| **Key properties** | status | Temp [°C] | | | | |
| **Thermal Conductivity, thru-thickness (W/m/K)** | | | | | | |
| | Non irradiated | 500 | <2 | ~15 | 25-40 | 15-40 |
| | Non Irradiated | 1000 | n/a | ~10 | 20-3 | 10-30 |

| | | | | | | |
|---|---|---|---|---|---|---|
| | Irradiated | 500 | <2 | 2-3 | 5-8 | - |
| | Irradiated | 1000 | n/a | 4-6 | 12-18 | - |
| **Tensile Properties** | | | | | | |
| **UTS [MPa]** | | 500-1000 | 300 | 250-350 | 100 | 300-400 |
| **MCS [MPa]** | | 500-1000 | n/s | ~150 | - | 200-250 |
| **E[GPa]** | | 500-1000 | 200-300 | ~250 | ~200 | 300-400 |

n/a: Not applicable; n/s: Not specified; -: Data not available

## 2. Economic benefits of PWR Cores with SiC cladding

Neutronic advantages of SiC cladding over up to now zirconium alloys permit to enhance the economic benefits of a NPP.

Three scenarios are discussed in M.S. Kazimi report (Kazimi, 2011):

- **Same power rate and same fuel length cycle:** SiC cladding allowance to have higher burn-up discharge rates and fewer loading fuel gives a margin of around 50.000$ of benefit per assembly, which may be dedicated to cover the manufacturing expenses of SiC claddings.
- **Up rated core power, 18 month cycle:** This changes affects both, fuel cost and generated energy. According to M.S. Kazimi, almost direct proportion is achieved, where a 10% of up rated generation gives 10M$ and 20% gives 20M$ of theoretical benefits but with a large variability depending on costs. It is important to keep in mind the investment necessary to allow the NPP to withstand this up rated energy production which may reduce the margin of benefits.
- **24 month cycle:** Results to be not economically viable. Main savings are in outage costs, since fuel reloads are less frequent. Although the outage savings, the need to augment the fresh assemblies inserted and discharging them with lower burn-up levels, makes SiC fuel costs greater than zirconium alloy ones.

Then, although major residence times or high power rates are feasible, the change to CMC claddings will not be performed unless they represent a real advantage in front of the zirconium alloy ones, being the benefit economic or a security improvement without affecting the profitability of a NPP.

# Annex 3

## TRIPLEX Properties Analysis

Mechanical test were made with two TRIPLEX cladding prototypes, one of them irradiated, via internal pressurisation at room temperature.

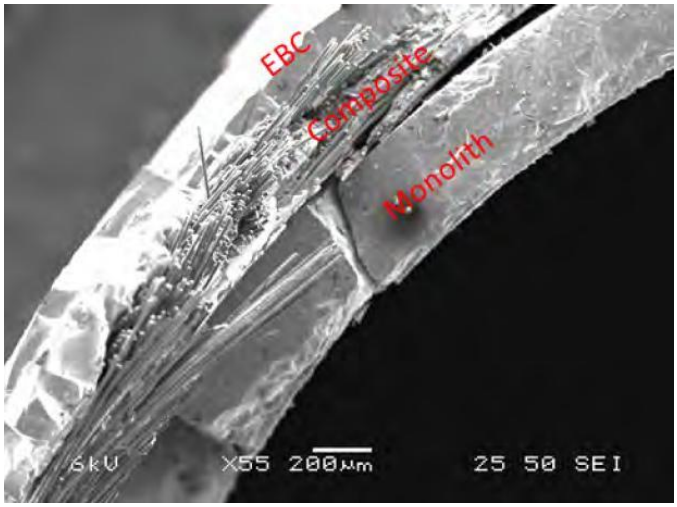


**Figure 33. Initial monolith layer crack and propagation to composite. Substantial debonding.**

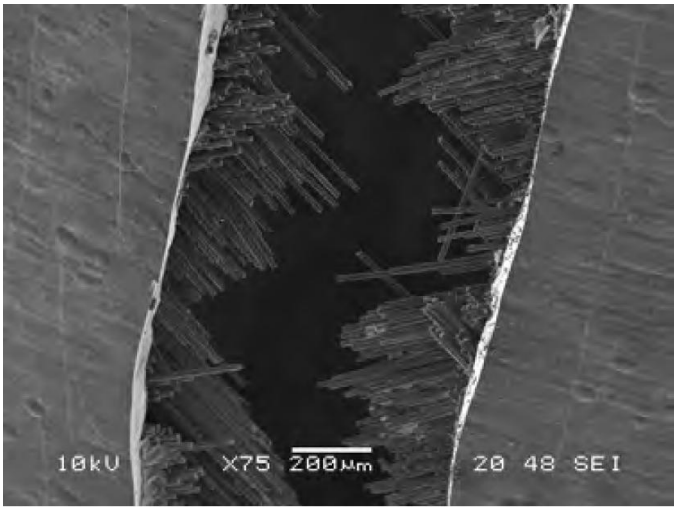


**Figure 34. Axial crack and fiber pul-out.**

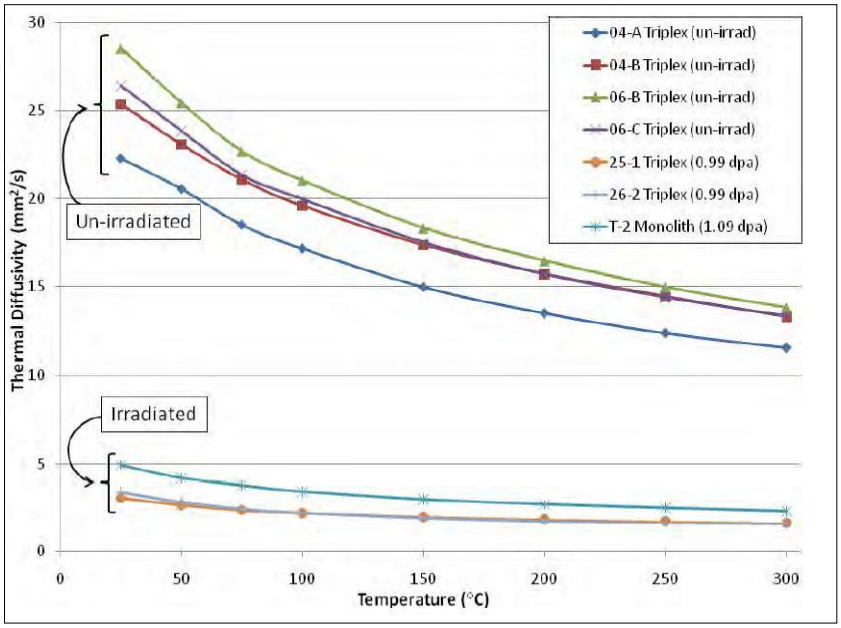


**Figure 35 Thermal diffusivity. Irradiated vs. Non irradiated SiC Triplex samples.**

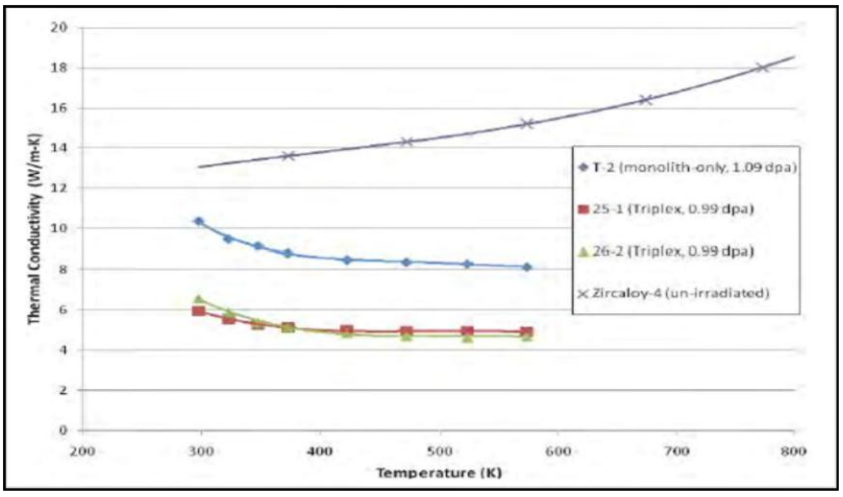


**Figure 36. Thermal conductivity of SiC monolith vs. Zircaloy-4**

Nevertheless the decrease of the thermal conductivity of the SiC/SiC due to irradiation, as the Zr alloys heat conductivity decrease due to corrosion, at long term both conductivities may reach same order of magnitude. (Stempien, Carpenter, Kohse, & Kazimi, 2011)

It is remarkable also that modelling of the behaviour of ceramic composite is not well developed and the existing approaches do not give reliably predictive data. The absence of data on nuclear applications of $SiC_f$/SiC CMC makes even harder this duty and a database of this material must be developed and populated. (Lahoda, Johnson, & Ray, 2011)

# Annex 4

## Licos input data from Alcyone results (fragment).

| Time [h] | Pint [MPa] | Vol Power [W/m$^3$] | TextClad [K] | $\varphi_{fast}$ [n/m$^2$/s] | Fluence [n/m$^2$] | $dpa_{SiC}$ |
|---|---|---|---|---|---|---|
| 21600 | 3.469722 | 77339383.21 | 567.79105 | 0.00E+00 | 0 | 0 |
| 43200 | 3.765613 | 154215417.7 | 576.170008 | 0.00E+00 | 0 | 0 |
| 64800 | 3.998512 | 230593135.2 | 583.3884 | 0.00E+00 | 0 | 0 |
| 86400 | 4.231565 | 306350412.7 | 590.947957 | 0.00E+00 | 0 | 0 |
| 108000 | 4.466358 | 381422278.1 | 598.470202 | 7.80E+17 | 8.424E+21 | 0.00206388 |
| 1639533 | 4.609193 | 380898631.2 | 598.684013 | 7.80E+17 | 1.2030196464E+24 | 0.031331473 |
| 3171066 | 4.645222 | 381032983.2 | 598.077672 | 7.80E+17 | 2.3976152928E+24 | 0.060599067 |
| 4702599 | 4.698237 | 381076043 | 598.151835 | 7.80E+17 | 3.5922109392E+24 | 0.08986666 |
| 6234132 | 4.750876 | 381107923.2 | 598.239262 | 7.80E+17 | 4.7868065856E+24 | 0.119134253 |
| 7631240 | 4.792363 | 381144655.6 | 598.2894 | 7.80E+17 | 5.87655139968E+24 | 0.145833001 |
| 9028349 | 4.832835 | 381169830.6 | 598.329199 | 7.80E+17 | 6.96629621376E+24 | 0.172531749 |
| 10464835 | 4.874204 | 381187920.9 | 598.374138 | 7.80E+17 | 8.0867552688E+24 | 0.199982996 |
| 11901321 | 4.91411 | 381204706.8 | 598.4127 | 7.80E+17 | 9.207214326648E+24 | 0.227434243 |
| 13150367 | 4.945683 | 381228209 | 598.444181 | 7.80E+17 | 1.01814704784E+25 | 0.251303519 |

$$\boldsymbol{P_{vol}[i]\left[\frac{W}{m^3}\right] = P_{lin}[i]\left[\frac{W}{m}\right] \cdot (\pi \cdot r[i]^2)^{-1}}$$

$$\boldsymbol{\varphi_{fast}[i][\frac{n}{(m^2 \cdot s)}] = \varphi_{Alc}[\frac{n}{m \cdot J}] \cdot P_{lin}[\frac{W}{m}]}$$

$$\boldsymbol{Fluence[i+1] = Fluence[i] + \frac{(\varphi_{fast}[i+1] + \varphi_{fast}[i])}{2} \cdot [t[i+1] - t[i]]}$$

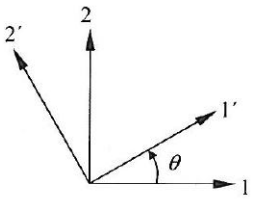


$$\overline{e_1'} = \begin{Bmatrix} \cos\theta \\ sen\theta \end{Bmatrix}_{1,2} \qquad \overline{e_2'} = \begin{Bmatrix} -sen\theta \\ \cos\theta \end{Bmatrix}_{1,2}$$

$$[R] = \begin{bmatrix} \cos\theta & -sen\theta \\ sen\theta & \cos\theta \end{bmatrix}$$

$$[\sigma']_{1',2'} = [R]^T [\sigma]_{1,2} [R]$$

$$\begin{cases} \sigma_{11}' = \dfrac{\sigma_{11}+\sigma_{22}}{2} + \dfrac{\sigma_{11}-\sigma_{22}}{2}\cos 2\theta + \sigma_{12} sen2\theta \\ \sigma_{22}' = \dfrac{\sigma_{11}+\sigma_{22}}{2} - \dfrac{\sigma_{11}-\sigma_{22}}{2}\cos 2\theta - \sigma_{12} sen2\theta \\ \sigma_{12}' = \sigma_{12}\cos 2\theta - \dfrac{\sigma_{11}-\sigma_{22}}{2} sen2\theta \end{cases}$$

In order to take into account the expansion, cylindrical geometry is supposed to remain constant. Then, taking the total length and dividing it by θ= 22.5º we obtain the actual radius, $R_T$ , intended to be $R_T \approx R_0 \cdot \alpha \cdot \Delta T$

For a length i: $\theta_i = l_i / R_T$, is the angle used in the computation.

# Annex 5

## Licos & Alcyone: points of calculation.

Licos 2D and Alcyone differ in the point of the pellet that they use for the calculus. While licos is calculating the medium symmetry plane of the pellet, Alcyone allows to calculate in both, inter pellet plane or inter-medium pellet planes.

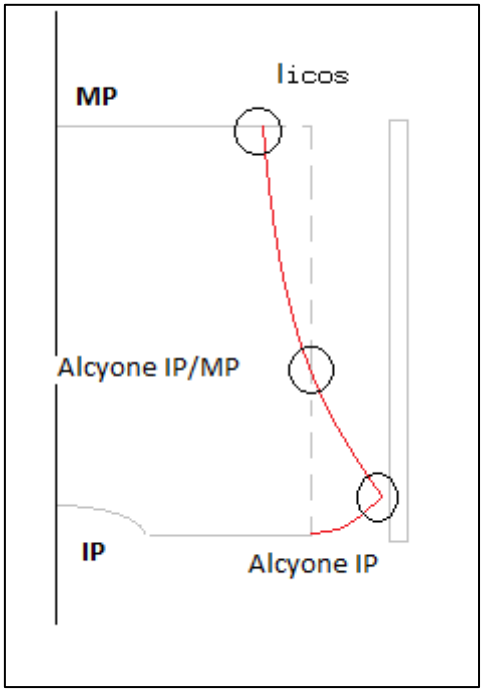


Figure 37 Alcyone & licos points of calculation

The different point of calculation implies some differences in the results. As the point of calculation of Alcyone is closer to the cladding, this will always have more interaction with the gain than de medium plane. This interaction affects thermal expansion behaviour, being minor in licos than in Alcyone due to the larger residual gap.

# Annex 6

## Alcyone and licos SiC Irradiation Swelling phenomenon

### Alcyone

Simplified analysis is carried out to identify the cause of the errors in the computation. The conditions used for the calculation in Alcyone were:

- Non gradient temperature or pressure between the inner and outer face of the cladding. This will avoid the creep effect and the thermal expansion.
- No fuel power. Neutronic damage is given.
- Forced room temperature at the cladding.

Under these work conditions, irradiation swelling phenomena is isolated.
What is observed is:

1.- At firsts steps, a sudden increase of both inner and outer radius of the cladding. This abrupt growth does not seem to be related to any physical phenomena.

2.- After the initial growth, a exponential decrease of the radius. Is remarkable that both; inner and outer radius, are saturating at the respective initial values (Ro=4.745 mm, Ri=4.12 mm)

3.- The saturation point corresponds to the one expected with the swelling law. This corresponds to 5000h approx (~0.4dpa)

4.- The radial deformation at 20°C should be around 1.2% while, considering the max. value reached at the beginning of the simulation, 0.4% is achieved.

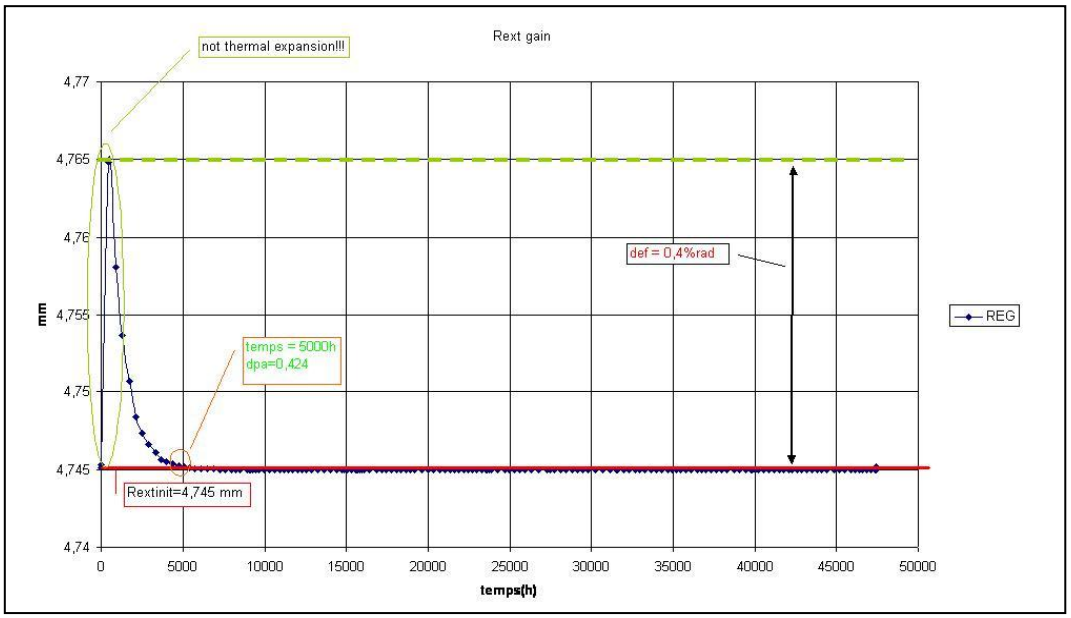


**Figure 38 Alcyone results: Isolated swelling phenomena.**

Notice that the saturation point is the one expected using the analytical evolution law, this law appears to be implemented in the code. Nevertheless, the errors observed in the Alcyone

computation point to a bad treatment of the results. Intent to reproduce the `Alcyone` bad response is done to see where could be the problem:

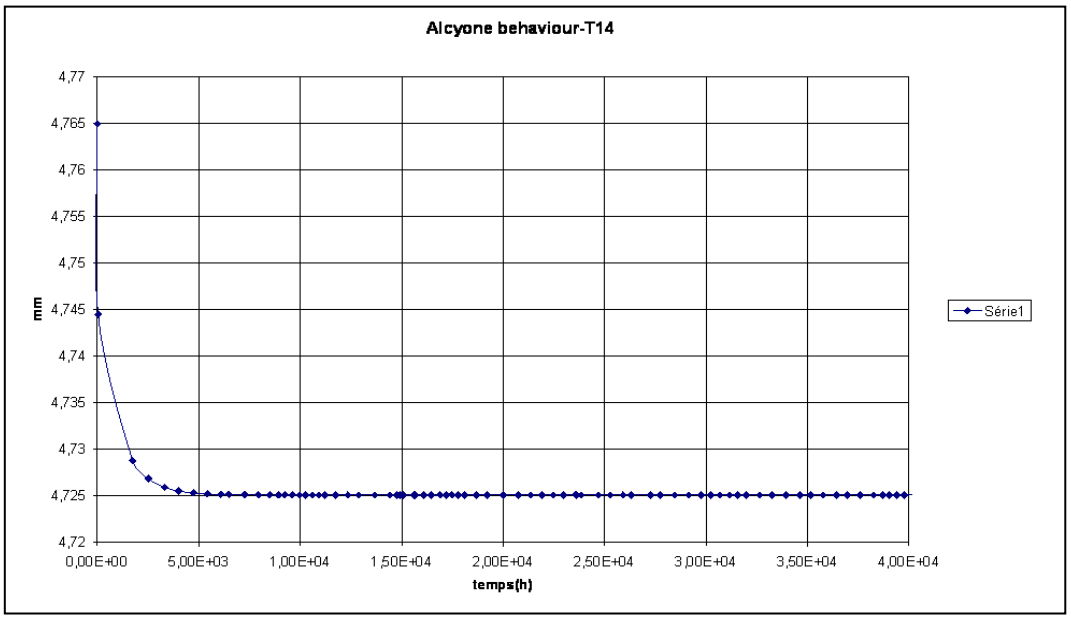


**Figure 39 Simulation of the `Alcyone` response using the theoretical law.**

This last graphic is obtained by considering a negative Gsat and giving as first value the initial radius multiplied by the saturation swelling. It may mean that at the end of the iterative process; the variable “gonfprec” may not be reassigned to cero. Also it may be noticed that the results are divided by a factor of three, this points to that maybe the transformation from volumetric to linear swelling (isometric) is done twice, giving the final result divided by 9.

### licos

Equal test has been performed to `licos`. Only the clad geometry has been tested here using the same boundary conditions than before.

SiC swelling phenomena present some differences with the analytical value.

As can be observed, SiC swelling between `licos` and the analytical law have parallel evolution but different saturation values.

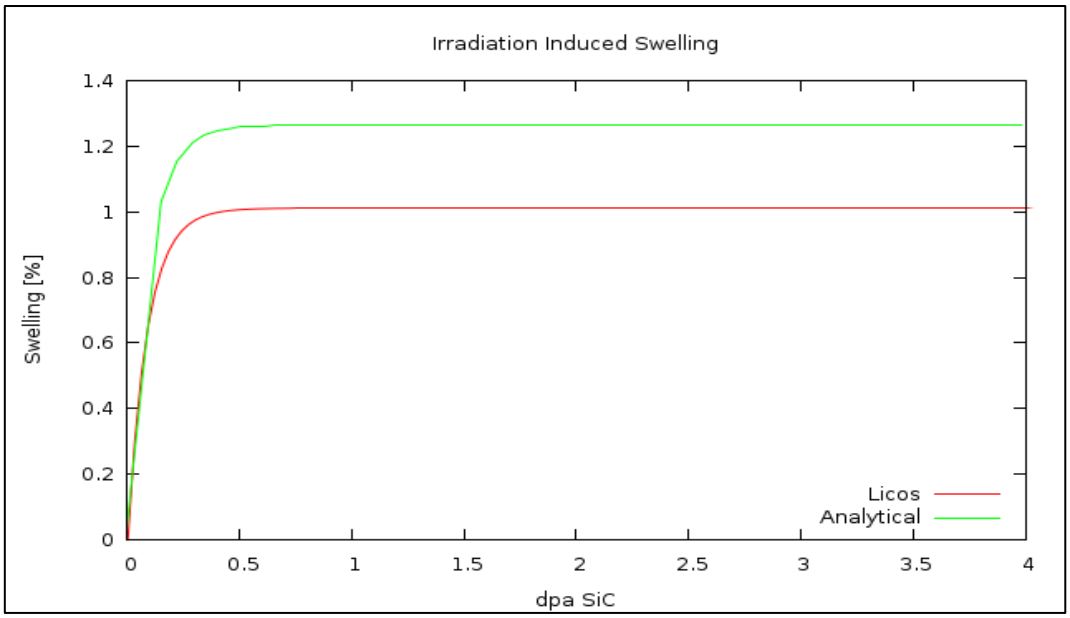


Figure 40 SiC swelling. `licos`-vs-analythic law

SiC `licos` irradiation induced swelling model has been modified using the swelling saturation constant law given in MZ-NT-SESC-11-006.

`Licos` results obtained with the modified model are now consistent.

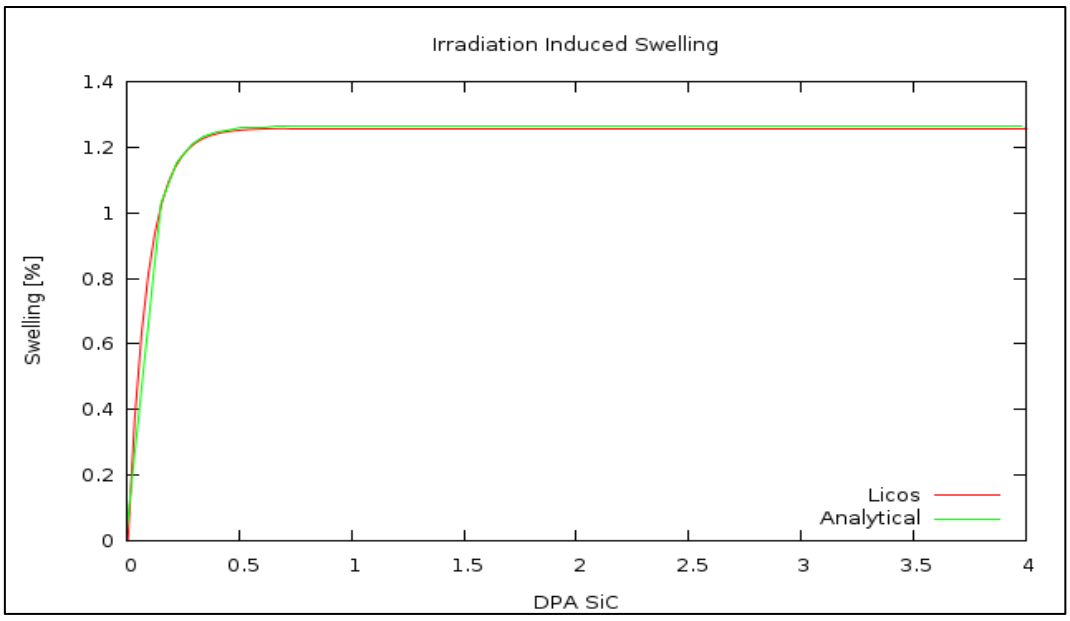


Figure 41 SiC swelling. `licos` modified Irr. Ind. Swell. model.

SiC volumetric swelling induced by fast neutron irradiation (Zabiego, Data for the GFR pin design, 2011, pp. 9-10):

$$S_{vol}^{n+1} = S_{vol}^{n} + \max\{0; (S_{sat}^{n} - S_{vol}^{n}) \cdot (1 - e^{-\frac{(\varphi_{fast}^{n+1} - \varphi_{fast}^{n})}{\varphi_0}}) \}$$

$$S_{vol}^{n} = \ vol.\ swelling\ [\%\text{vol}] \text{ at time tn}$$

$S_{sat}^{n} = swelling\ saturation\ constant\ [vol\%] at\ time\ tn\ at\ temperature\ T[℃]$

$$S_{sat}^{n} = 4 \cdot e^{-Tn/370}$$

$$\varphi_{fast}^{n} = \ fast\ fluence\ at\ time\ tn$$

$$\varphi_0 = 3.396 \cdot 10^{24}\ \frac{n_{fast}}{m^2}\ .Fast\ fluence\ constant. Controlls\ the\ saturation\ kinetics.$$

Cumulative dose, $dpa_{SiC}$ is used rather than the fast fluence. Equivalence can be considered as:

$$10^{25}\frac{n}{m^2} \approx 0.6\ dpa_{SiC}$$

# Annex 7

## Previous studies of CMC claddings: Monolayer, Duplex and Sandwich

### Monolayer $SiC_f/SiC$ Cladding

`Alcyone` studies reveal (Zabiego, 2011):

- Gap closure is leaded by fuel swelling instead of cladding's creep.
- Under PCMI conditions stresses in the cladding overpass the elastic limit of the CMC.
- Primary stresses: favourable in nominal conditions but potential problem in case of depressurisation. (Pint>Pext → cladding under traction)
- Irradiation induced swelling in the cladding. In case of power shutdown cancellation of thermal stresses may result into a strong action of the non-compensated swelling differential swelling stresses.

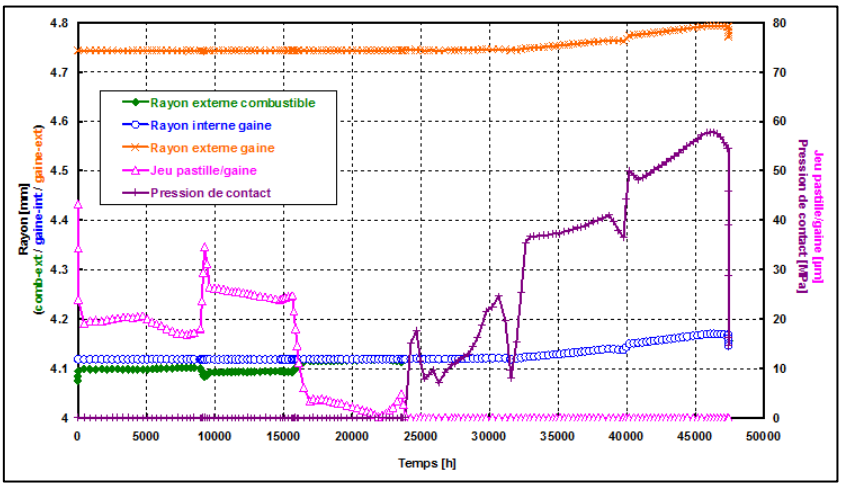


Figure 42 Monolayer CMC Cladding: Fuel-Cladding Radial Evolution (wo swelling)

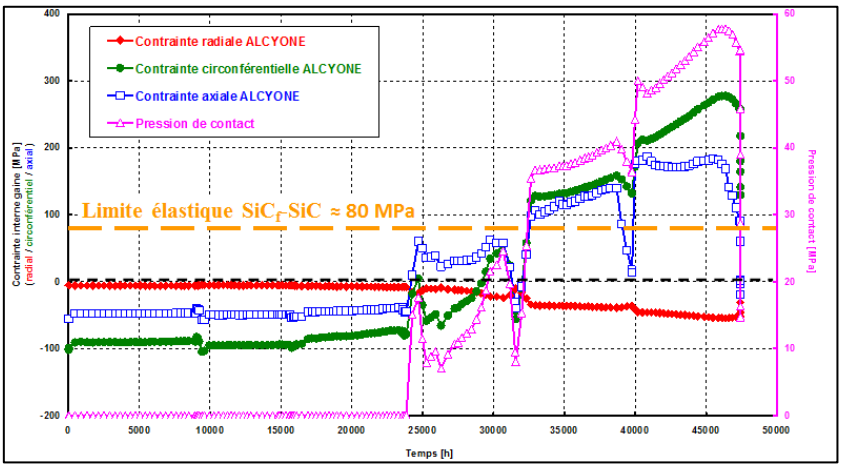


Figure 43 Monolayer CMC Cladding: Mechanical Constraints (wo cladding swelling)

Note that in previous calculations `Alcyone` $SiC_f/SiC$ swelling model is not yet implemented.

## Duplex Cladding: monolithic SiC- $SiC_f/SiC$

To solve the leak tightness of a monolayer CMC cladding, The Duplex design was proposed (Pelletier, 2010). It is composed of an inner-layer of monolithic SiC to ensure the tightness of the cladding and one external layer of SiCf/SiC to enhance the mechanical properties.

`Licos` studies over Duplex reveal (RENAUD, 2011):

- No PCMI due to the irradiation induced swelling in the cladding. (see Figure 21)
- Cladding remains under compression during in-core residence.
- Differential thermal stresses compensated by cladding's swelling. During a stop thermal stresses cancellation restores swelling stresses to maximum value.

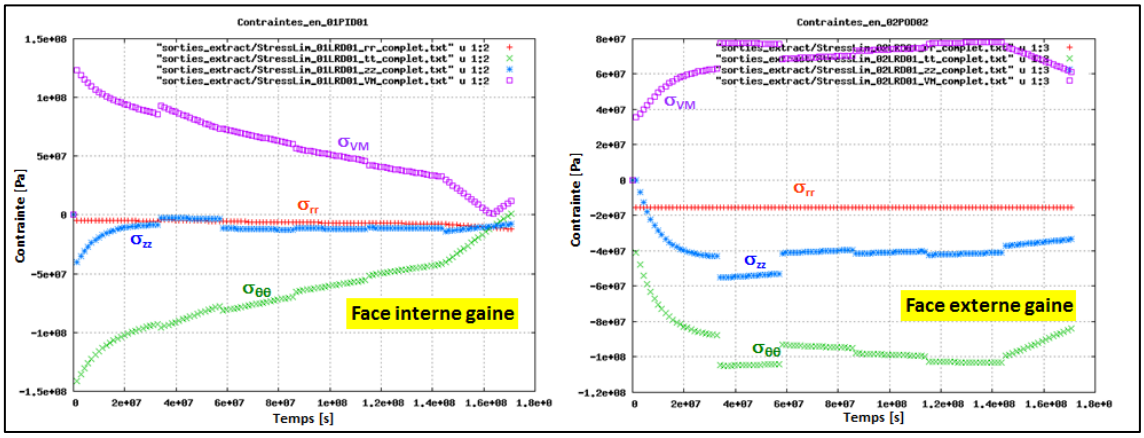


Figure 44 Duplex: Mechanical Constraints.

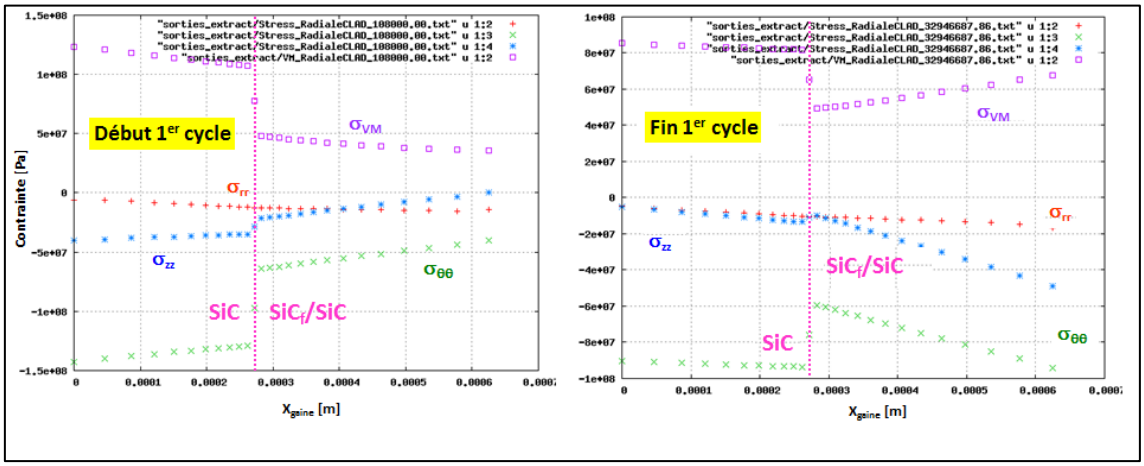


Figure 45 Duplex: Radial Evolution of Tensions during the first irradiation cycle

## SANDWICH

Preliminary SANDWICH studies have been performed with the structure mentioned below:

Table 6 SANDWICH: Preliminary studies' geometry

| | Material | Thickness (μm) |
|---|---|---|
| Inner layer | $SiC_f/SiC$ | 250 |
| Metallic liner | Nb-1Zr-0.1C | 100 |
| Outer layer | $SiC_f/SiC$ | 250 |

NbZrC alloy presents the refractory characteristics mentioned in **Error! Reference ource not found.**

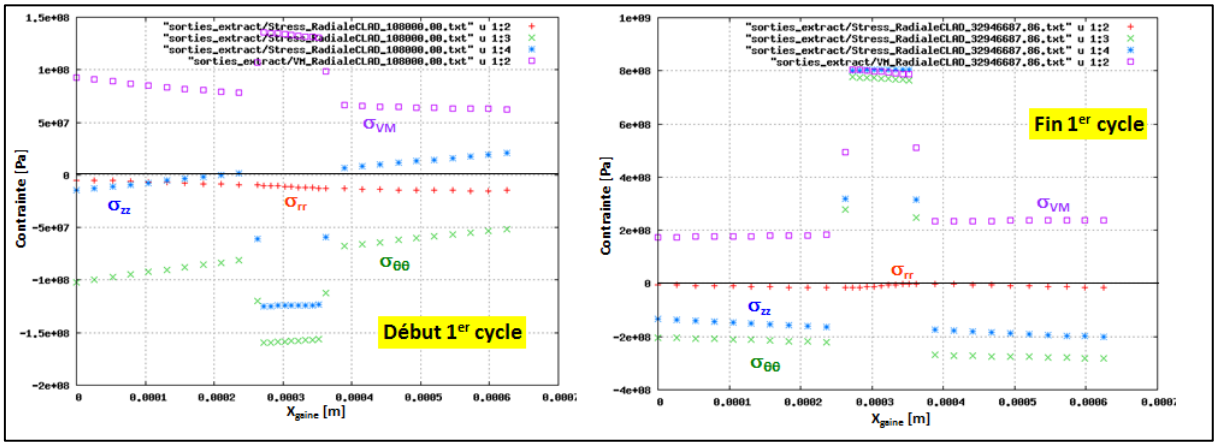


Figure 46 SANDWICH: Preliminary results

Preliminary results show the stresses at beginning of the first irradiation cycle caused by the different thermal expansion of both materials. The metallic liner tends to expand more rapidly than CMC ($\alpha_{SiC}=4\cdot10^{-6}\,[K^{-1}]$ $\alpha_{NbZrC}=6\cdot10^{-6}\,[K^{-1}]$). Internal and external $SiC_f/SiC$ layers have a low capability to adapt to the liner's thermal expansion causing its compression. Nevertheless this fact does not suppose any limiting problem it is necessary to study the behaviour of the cladding during the power transient.

In opposition to this initial compressive state of the metallic liner, at the end of the irradiation cycle and due to the irradiation induced swelling, liner goes to an excessive traction state, up to 800 MPa.

This last result was not taking in account the possible stress relaxation due to plasticity as the `licos` NbZrC mechanical model is only characterised in the elastic region.

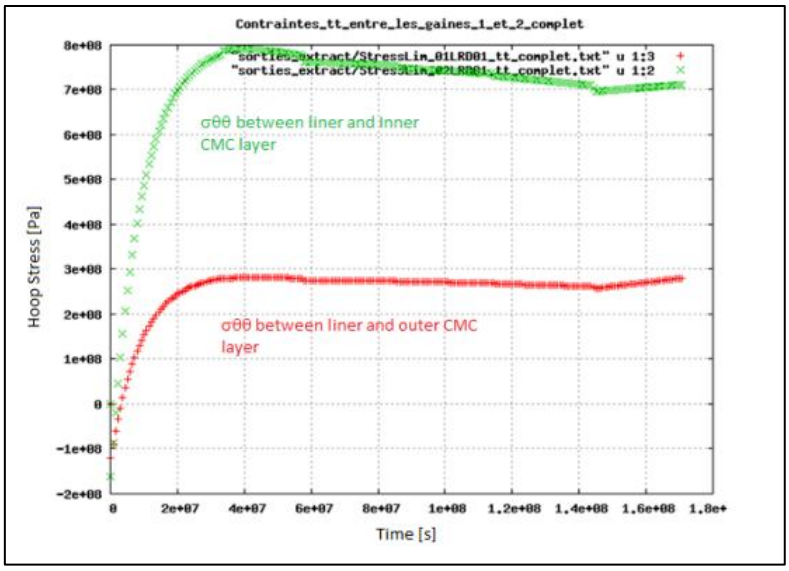


**Figure 47 SANDWICH preliminary results: SiC swelling effect over metallic liner**

# Annex 8

## licos reference case input deck

```
Mesh 'mesh/meshdata.med'
CastemMeshDensity 1.e-12
CastemMemoryManagementPolicy 'LowMemoryUsage'
ModellingHypothesis 'GeneralisedPlaneStrain'

Int OutputFile.Precision 15

Materials {'FUEL','GAS','CLAD1','CLAD2','CLAD3'}


GeneralisedPlaneStrainReferencePoints
{'FUEL':'pFUEL','GAS':'pGAS','CLAD1':'pCLAD','CLAD2':'pCLAD','CLAD3':'pCLAD'}



// ------------------------------------------------------------------------------
// Librairies standard licos
// ******************************************************************************


ExternalLibrary 'libPleiadesStandardModels.so'
ExternalLibrary 'libUO2MaterialProperties.so'
ExternalLibrary 'libUO2MaterialModels.so'
ExternalLibrary 'libSiCMaterialModels.so'
ExternalLibrary 'libM5MaterialModels.so'
ExternalLibrary 'models/SiC_IrradiationSwellingModel/src/libLicosSiCModels.so'
ExternalLibrary 'models/FuelGaseousSwelling/src/libLicosMaterialModels.so'

// ******************************************************************************
// Matériaux
// ******************************************************************************

// ---------------------------------------- Combustible

Import 'UO2.ple'

Material<UO2DDIF2> 'FUEL'
MaterialProperty<constant> 'Porosity'  0.05
MaterialProperty<constant> 'GrainSize' 8e-6
  MaterialProperty<constant> 'FractureStress0'     1.e20
  MaterialProperty<constant> 'FractureStress1'    136.e6
  MaterialProperty<constant> 'FractureStress2'    136.e6
  MaterialProperty<constant> 'SofteningModulus0'   -75.e9
  MaterialProperty<constant> 'SofteningModulus1'   -75.e9
  MaterialProperty<constant> 'SofteningModulus2'   -75.e9
  MaterialProperty<constant> 'GrainsSpecificSurface' 530973.45

EndOfMaterial


// ---------------------------------------- Gaine2: M5


CastemNames {'PowerRampTest' : 'PRAM'}

Import 'M5_ZO-REFLET.ple'
Material<M5Orthotropic> 'CLAD2'
AnisotropicAxises {'x','y'}
EndOfMaterial


// ---------------------------------------- Gaine1 et Gaine3 (CMCortho)

ExternalLibrary 'libSiCMaterialModels.so'
Import 'SiCSiCmodels/RCMY_T2D3C09_JH.ple'
Import 'SiCSiCmodels/RCMY_E303C_JH.ple'


Material<RCMY_E303C> {'CLAD1'}
```

```
 AnisotropicAxises {'x','y'}
EndOfMaterial

Material<RCMY_T2D3C09> {'CLAD3'}
 AnisotropicAxises {'x','y'}
EndOfMaterial

// ---------------------------------------- Gaz

GaseousMaterial 'GAS'

ChemicalSpecies {'Helium','Nitrogen','GaseousFissionProducts'}

MaterialProperty<constant> 'MassDensity' 0.

StateVariable 'Pressure'                          1.60e6
StateVariable 'HeliumMolarRatio'                  0.999
StateVariable 'NitrogenMolarRatio'                0.001
StateVariable 'GaseousFissionProductsMolarRatio'  0.

EndOfGaseousMaterial

// ********************************************************************************
// Modèles
// ********************************************************************************


// ********************************************************************************
// Conditions aux limites
// ********************************************************************************
// ---------------------------------------------------------------
// Blocages mécaniques


MechanicalLoading<Contact> {'00COOD':'01COID'}
AxialBinding true
CoulombFrictionCoefficient 0.47
EndOfMechanicalLoading


MechanicalLoadings


  ML<ImposedGeneralizedPlaneStrainRotation>

  ML<SymmetryLine> {'00LRD01'}
  ML<FractureLine> {'00LRD02'}

ML<ImposedDisplacement> {'00PID00'} {'UX','UY'}

  ML<SymmetryLine> {'RCLAD01'}
  ML<SymmetryLine> {'RCLAD02'}

  ML<Swelling> 'FUEL' using Field 'SolidSwelling'
  // ML<Swelling> 'FUEL' using Field 'GaseousSwelling_ext'
  ML<Swelling> 'FUEL' using Field 'GaseousSwelling_int'

ML<ImposedPressure> '03COOD' using LoadingEvolution 'ExternalPressure'
ML<ImposedPressure> '00COOD' using LoadingEvolution 'InternalPressure'
ML<ImposedPressure> '01COID' using LoadingEvolution 'InternalPressure'

  //ML<GasPressure> 'GAS'

  ML<Swelling> 'CLAD1' using Field 'IrradiationInducedSwelling'
  ML<AxialSwelling> 'CLAD2' using Field 'IrradiationSwelling'
  ML<Swelling> 'CLAD3' using Field 'IrradiationInducedSwelling'

EndOfMechanicalLoadings

MechanicalLoading<EndCapEffect>
  CladdingMaterials {'CLAD1','CLAD2','CLAD3'}
EnclosedMaterials {'FUEL', 'GAS'}
  InnerPressure using LoadingEvolution 'InternalPressure'
  OuterPressure using LoadingEvolution 'ExternalPressure'
EndOfMechanicalLoading
```

```
// ------------------------------------------------------------
// Conditions limites de temperature

ThermalLoadings

    TL<HeatSource> 'FUEL' using LoadingEvolution 'FUELPower'
    TL<ImposedTemperature> '03COOD' using LoadingEvolution 'ExternalTemperature'

EndOfThermalLoadings

ThermalLoading<GasHeatTransfer> 'GAS'
  HeatTransferCoefficient<castem> 'properties/src/libCastemGas.so' 'Gas_HeatTransfer'
EndOfThermalLoading

// ********************************************************************************
// Couplage
// ********************************************************************************

ExternalLibrary 'libPleiadesPythonAuxiliaryTask.so'

Coupling 'LoopCoupling' 1
 SpecialisedAuxiliaryTask 'PythonAuxiliaryTask'
    String Module 'AzimuthAngle'
    String Class  'AzimuthAngle'
  EndOfSpecialisedAuxiliaryTask
  Model 'FissionDensityModel'
  Model 'LicosBurnUpModel'
  Model 'UO2_CombustionMassique'
  Model 'UO2_SolidSwellingModel'
  Model 'FuelExternalGaseousSwelling'
  Model 'FuelInternalGaseousSwelling'
  Model 'GasCompositionModel'
  Model 'CastemThermalModel' {'FUEL','CLAD1','CLAD2','CLAD3'}
  Model 'M5_IrradiationSwellingModel' {'CLAD2'}
Model 'SiC_IrradiationSwellingModel_2' {'CLAD1','CLAD3'}

 SpecialisedModel 'CastemMechanicalModel' {'FUEL','CLAD1','CLAD2','CLAD3'}

    String ResolutionProcedure 'INCREPL'
    Bool   AllowForcedConvergenceAlgorithm true
    Double Precision      1.e-3
    Bool LargeDisplacement true
    Bool UpdateMeshCoordinates true


  EndOfSpecialisedModel

SpecialisedModel 'PythonModel'

     String Module 'SiCSiC_SigmaFailure'
     String Class  'SiCSiC_SigmaFailure'

   EndOfSpecialisedModel

EndOfCoupling

// ********************************************************************************
// Chargements
// ********************************************************************************

Double tramp 21848936

   Loading<Uniform> PowerRampTest {'CLAD1','CLAD2','CLAD3'}
   Function 'H(t-tramp)'
   EndOfLoading

// ------------------------------------------------------------------------------
// Conditions aux limites de température et pression

LoadingEvolutionFromTextFile ExternalTemperature 'Donnees_Rampe_SansContact.txt' 1 4
UniformLoadingFromEvolution ExternalTemperature 'ExternalTemperature'

LoadingEvolutionFromTextFile InternalPressure 'Donnees_Rampe_SansContact.txt' 1 2
UniformLoadingFromEvolution InternalPressure 'InternalPressure' {'00COOD','01COID'}
```

```
LoadingEvolution<Table>

Time          ExternalPressure
  00              155e5
  170741963       155e5
EndOfLoadingEvolution

UniformLoadingFromEvolution ExternalPressure 'ExternalPressure'

CastemNames {'NeutronFluence' : 'FLUE'}

// ------------------------------------------------------------------------
// Chargements de Puissance
// ---------------------------------------- Puissance uniforme dans la gaine

LoadingEvolutionFromTextFile FUELPower 'Donnees_Rampe_SansContact.txt' 1 3
UniformLoadingFromEvolution FUELPower 'FUELPower' 'FUEL'


// ------------------------------------------------------------------------
// Chargements de Fluence
// ---------------------------------------- Puissance uniforme dans la gaine
LoadingEvolutionFromTextFile EvolFlux 'Donnees_Rampe_SansContact.txt' 1 5

UniformLoadingFromEvolution FastNeutronFlux 'EvolFlux' {'FUEL','CLAD1','CLAD2','CLAD3'}

LoadingEvolutionFromTextFile EvolFluence 'Donnees_Rampe_SansContact.txt' 1 6

UniformLoadingFromEvolution FastNeutronFluence 'EvolFluence'
{'FUEL','CLAD1','CLAD2','CLAD3'}

// ---------------------------------------- Dose

LoadingEvolutionFromTextFile EvolDose 'Donnees.txt' 1 7
UniformLoadingFromEvolution IrradiationDamage 'EvolDose' {'CLAD1','CLAD2','CLAD3'}


// ------------------------------------------------------------------------
// Imposed Gaseous Swelling from Alcyone
// ----------------------------------------GaseousSwelling

LoadingEvolutionFromTextFile MeanGaseousSwelling_ext
'data/GaseousSwellingFromAlcyone_rad.dat' 1 2
UniformLoadingFromEvolution MeanGaseousSwelling_ext 'MeanGaseousSwelling_ext'

Loading<Kriging> RadialGasSwellDistribution_ext 'FUEL'
  SpatialVariable 'r'
  TextData 'data/distr_radial_swell_ext.dat' {'r': 1,'RadialGasSwellDistribution_ext':
2}
EndOfLoading


LoadingEvolutionFromTextFile MeanGaseousSwelling_int 'data/GasSwellAlc_int.dat' 1 2
UniformLoadingFromEvolution MeanGaseousSwelling_int 'MeanGaseousSwelling_int'

Loading<Kriging> RadialGasSwellDistribution_int 'FUEL'
  SpatialVariable 'r'
  TextData 'data/distr_radial_swell_int.dat' {'r': 1,'RadialGasSwellDistribution_int':
2}
EndOfLoading


// ------------------------------------------------------------------------
// Description temporelle
// ------------------------------------------------------------------------
// Temporal discretisation from Alcyone IrradHist


Import 'Times_Rampe_SansContact.ple'

// ------------------------------------------------------------------------
// Post traitements
// ------------------------------------------------------------------------
Curve 'IrradiationInducedSwelling' '01PID01' in 'CLAD1'
'curves_rampe_sansContact/IrradIndSwelling.txt'
Curve<MeanValue> 'PowerDensity' 'FUEL' 'curves_rampe_sansContact/PowerDensity_FUEL.txt'
Curve<TVector> 'Displacement' '00POD01' in 'FUEL' 'curves_rampe_sansContact/disp.txt'
```

```
Curve 'BurnUp' '00PID00' 'curves_rampe_sansContact/BurnUp_00PID00.txt'
Curve 'CombustionMassiqueMetal' '00PID00' 'curves_rampe_sansContact/BurnUp_CMM.txt'
Curve 'GaseousFissionProductsMolarRatio' '00POD01' in 'GAS'
'curves_rampe_sansContact/GaseousFissionProductsMolarRatio.txt'
Curve 'HeliumMolarRatio' '00POD01' in 'GAS'
'curves_rampe_sansContact/HeliumMolarRatio.txt'
Curve 'NitrogenMolarRatio' '00POD01' in 'GAS'
'curves_rampe_sansContact/NitrogenMolarRatio.txt'

MultipleCurves 'curves_rampe_sansContact/Pressure.txt'
Curve 'Pressure' '00POD01' in 'GAS'
Curve 'Pressure' '01PID01' in 'GAS'

EndOfMultipleCurves

MultipleCurves 'curves_rampe_sansContact/Temperatures.txt'
Curve 'Temperature' '00PID00' in 'FUEL'
Curve 'Temperature' '00POD01' in 'FUEL'
Curve 'Temperature' '01PID01' in 'CLAD1'
Curve 'Temperature' '03POD01' in 'CLAD3'
EndOfMultipleCurves
MultipleCurves 'curves_rampe_sansContact/Stress.txt'
Curve<Stensor> 'Stress' '00PID00' in 'FUEL'
Curve<Stensor> 'Stress' '00POD01' in 'FUEL'
Curve<Stensor> 'Stress' '01PID01' in 'CLAD1'
Curve<Stensor> 'Stress' '02PID01' in 'CLAD2'
Curve<Stensor> 'Stress' '02POD01' in 'CLAD2'
Curve<Stensor> 'Stress' '03POD01' in 'CLAD3'
EndOfMultipleCurves
// ------------------------------------------------------------------------

LineCurve 'Temperature' 'Rayon' 'curves_rampe_sansContact/Temp_Rayon01.txt'

LineCurve 'VonMisesStress' '00LRD01' 'curves_rampe_sansContact/VM_FUEL.txt'
LineCurve<Stensor> 'Stress' '00LRD01' 'curves_rampe_sansContact/Stress_FUEL.txt'

LineCurve 'VonMisesStress' '01LRD01' 'curves_rampe_sansContact/VM_CLAD1.txt'
LineCurve 'VonMisesStress' '02LRD01' 'curves_rampe_sansContact/VM_CLAD2.txt'
LineCurve 'VonMisesStress' '03LRD01' 'curves_rampe_sansContact/VM_CLAD3.txt'
LineCurve 'VonMisesStress' 'RCLAD01' 'curves_rampe_sansContact/VM_CLAD01.txt'
LineCurve 'VonMisesStress' 'RCLAD02' 'curves_rampe_sansContact/VM_CLAD02.txt'

LineCurve<Stensor> 'Stress' '01LRD01' 'curves_rampe_sansContact/Stress_CLAD1.txt'
LineCurve<Stensor> 'Stress' '02LRD01' 'curves_rampe_sansContact/Stress_CLAD2.txt'
LineCurve<Stensor> 'Stress' '03LRD01' 'curves_rampe_sansContact/Stress_CLAD3.txt'

LineCurve<Stensor> 'Stress' '01LRD02' 'curves_rampe_sansContact/Stress_CLAD1_02.txt'
LineCurve<Stensor> 'Stress' '02LRD02' 'curves_rampe_sansContact/Stress_CLAD2_02.txt'
LineCurve<Stensor> 'Stress' '03LRD02' 'curves_rampe_sansContact/Stress_CLAD3_02.txt'


LineCurve<Stensor> 'Stress' '01COID' 'curves_rampe_sansContact/Stress_azym.txt'
// ------------------------------------------------------------------------

CastemGraphicalOutput 'Temperature' 'FUEL' 'graphs/FUELTemp.ps'
CastemGraphicalOutput 'Temperature' {'FUEL','CLAD'} 'graphs/FUELCLADTemp.ps'
CastemGraphicalOutput 'Temperature' {'CLAD'} 'graphs/CLADTemp.ps'

CastemGraphicalOutput 'VonMisesStress' {'FUEL'} 'graphs/VMFUEL.ps'
CastemGraphicalOutput 'VonMisesStress' {'CLAD1','CLAD2','CLAD3'} 'graphs/VMCLAD.ps'

CastemGraphicalOutput 'TrescaStress' {'FUEL'} 'graphs/TrescaFUEL.ps'
CastemGraphicalOutput 'TrescaStress' {'CLAD1','CLAD2','CLAD3'} 'graphs/TrescaCLAD.ps'



CastemGraphicalOutput 'Pressure' {'GAS'} 'graphs/Pressure_GAS.ps'
                                    //CastemGraphicalOutput 'ThermalStrain' {'FUEL'}
'graphs/FUELSTRAIN.ps'

// ------------------------------------------------------------------------

MPScriptIII<AllTimes,00POD01,01PID01,01POD01,03POD01> 'COORD_P' 'Coord_Point_2D.dgibi'
'curves_rampe_sansContact/Coord_Point_?.txt'

MultipleCurves 'curves_rampe_sansContact/coords.txt'
Curve 'UpdatedFirstCoordinate' '00POD01' in 'FUEL'
```

```
Curve 'UpdatedFirstCoordinate' '01PID01' in 'CLAD1'
Curve 'UpdatedFirstCoordinate' '01POD01' in 'CLAD1'
Curve 'UpdatedFirstCoordinate' '02PID01' in 'CLAD2'
Curve 'UpdatedFirstCoordinate' '02POD01' in 'CLAD2'
Curve 'UpdatedFirstCoordinate' '03PID01' in 'CLAD3'
Curve 'UpdatedFirstCoordinate' '03POD01' in 'CLAD3'

EndOfMultipleCurves

MechanicalPostProcessing<DeformedMesh> 'graphs/Cladding.ps'
Mesh 'CLAD'
DeformedMeshColor 'Red'
UnDeformedMeshColor 'TurquoiseBlue'
EndOfMechanicalPostProcessing



ScalarValueTransformation Damaged '(x>0) ? 1 : 0'
 CastemGraphicalOutput<Damaged> 'FailureCriteria' {'CLAD1','CLAD3'} 'graphs/damaged.ps'
 CastemGraphicalOutput 'SigmaFailure_SiC' {'CLAD1','CLAD3'} 'graphs/sigFailure_SiC.ps'
```

## [Abstract]

The use of a multi-layered ceramic based fuel clad for current PWRs nuclear power plants is studied.

The cladding design, thereafter *Sandwich*, is composed by three layers: one metallic liner enclosed between two ceramic SiC-based composites.

The aim of this study is to set a reference case for the thermo-mechanical analysis of the innovative cladding for a new finite elements design code.

With this purpose, benchmarking against the PWR reference code is performed to detect the validity of the results and it limitations.

Once that the reference case is set, the thermo-mechanical response of the *Sandwich* cladding under PWR conditions is evaluated and compared with previous studies.

This last evaluation emphasizes on its capacity to withstand nominal and accidental power transients as well as pellet cladding mechanical interaction.